Spring 5-8-2023

Atmospheric Carbon Capture: A Review on Current Technologies and Analysis of Energy Consumption for Various Direct Air Capture (DAC) Systems

Jennifer Perskin
Embry-Riddle Aeronautical University, perskinj@my.erau.edu

ATMOSPHERIC CARBON CAPTURE: A REVIEW ON CURRENT TECHNOLOGIES AND ANALYSIS OF ENERGY CONSUMPTION FOR VARIOUS DIRECT AIR CAPTURE (DAC) SYSTEMS

by

Jennifer Barri Perskin

A Thesis Submitted to the College of Engineering Department of Mechanical Engineering in Partial Fulfillment of the Requirements for the Degree of

Master of Science in Mechanical Engineering

Embry-Riddle Aeronautical University

Daytona Beach, Florida

May, 2023

ATMOSPHERIC CARBON CAPTURE: A REVIEW ON CURRENT TECHNOLOGIES AND ANALYSIS OF ENERGY CONSUMPTION FOR VARIOUS DIRECT AIR CAPTURE (DAC) SYSTEMS

by

Jennifer Barri Perskin

This thesis was prepared under the direction of the candidate's Thesis Committee Chair, Dr. Sandra Boetcher, Research Fellow and Professor of Mechanical Engineering, Daytona Beach Campus, and Thesis Committee Members Dr. Rafael Rodriguez, Associate Chair and Associate Professor of Mechanical Engineering, Daytona Beach Campus, and Claus Daniel, Ph.D., Carrier, and has been approved by the Thesis Committee. It was submitted to the Department of Mechanical Engineering in partial fulfillment of the requirements for the degree of Master of Science in Mechanical Engineering.

Thesis Review Committee:

Sandra Boetcher, Ph.D. Committee Chair, Mechanical Engineering	Rafael Rodriguez, Ph.D. Committee Member, Mechanical Engineering
Claus Daniel, Ph.D. Committee Member, Carrier	Jean-Michel Dhainaut, Ph.D. Graduate Program Chair, Mechanical Engineering
Jim Gregory, Ph.D. Dean, College of Engineering	Christopher Grant, Ph.D. Associate Provost
Patrick Currier, Ph.D. Department Chair, Mechanical Engineering	

Date

Acknowledgements

I would like to express my deepest gratitude to my advisors and committee members throughout my research and collegiate career. Dr. Boetcher, thank you for being my thesis advisor and for your invaluable patience and guidance throughout this process. Dr. Rodriguez, thank you for sparking my interest in the HVAC field, and for your vast wisdom and wealth of experience that has inspired me throughout my studies. Claus, thank you for your technical expertise, passionate participation, and input to this research. Thanks should also be given to the DAC research group led by Dr. Von Hippel for their continued support and contribution.

I am also grateful to my lab mates, classmates, and fellow graduate students for making my time at Embry-Riddle Aeronautical University like no other. Special shout-outs to Nick and Yang. Friends like you come once in a life-time and I'm excited to see you both do great things in life.

Lastly, I would like to thank my parents, Jo Ann and Jeffrey, my brother, Daniel, and my partner, Charles, for always believing in me and supporting me. And thank you to my cats, Rumi and Katsuji, for all the joy and comfort over the years.

Thank you all, this accomplishment would not have been possible without you.

Abstract

Researcher: Jennifer Barri Perskin

Title: Atmospheric Carbon Capture: A review on current technologies and analysis of energy consumption for various Direct Air Capture (DAC) systems

Institution: Embry-Riddle Aeronautical University

Degree: Master of Science in Mechanical Engineering

Year: 2023

Carbon dioxide (CO_2) capture is a crucial approach to reducing greenhouse gases in the atmosphere to directly combat climate change. Major components of the technology to desublimate CO_2 at cryogenic temperatures are mature and have the potential to be applied to build large Arctic/Antarctic direct-air CO_2 capture plants. Pressure swing adsorption another gas separation technique used in industry today that can be modified for atmospheric carbon capture. The discussion of energy consumption for cryogenic and combined direct air capture systems is explored in this study. The investigation of precompression of atmospheric air for a direct-air capture CO_2 system using an attached "waste-cool" precooler is examined. In this novel approach, a thermodynamic model based on psychrometric theories is evaluated to determine the required work input of the system at various inlet compression ratios and various inlet temperatures. Turbine recovery is also considered for the potential to capture "waste energy." A pressure swing adsorption unit is evaluated as another modification to the cryogenic system to minimize energy consumption.

Table of Contents

Page

Thesis Review Committee i

Acknowledgements ii

Abstract iii

List of Tables vi

List of Figures vii

Chapter

I Introduction 1

Significance of the Study 1

Statement of the Problem 10

Purpose Statement 10

Scope of Study 12

Limitations 12

Variables 13

Greek Letters 14

Definition of Terms 15

List of Acronyms 15

II Literature Review 17

Sorbent Material for DAC 17

Desired Sorbent Characteristics 20

Well Performing Sorbents for DAC 21

Cryogenic Arctic/Antartic DAC 24

Pressure Swing Adsorption DAC 28

III Methodology 35

Energy Analysis: Precompression of Atmospheric Air 35
System Model Overview 35
Compressor and Recovery Turbine 38
Precooling Heat Exchanger 40
Deposition Chamber 40
Cryogenic Refrigeration Cycle 40
Thermal Properties and Analysis 41
Energy Analysis: Pressure Swing Adsorption 44
System Model Overview 44
System Model Assumptions 45
Ideal Gas System Model 46
Conservation of Energy 47
Pressure Drop in the PSA Chamber 48
Adsorption Temperature 48
Adsorption Isotherms 49
Work per CO_2 Captured Basis Conversion 53

IIII Results 54
Energy Benefit of Precompression for Cryogenic DAC 54
PSA Combination DAC 61

V Conclusions 67
Future Recommendations 68

References 70

List of Tables

Page

Table

1.1 EV Market share as a percentage of total vehicle sales in that country per year from 2013-2020. Most countries have seen an increase in EV sales over time. Data adapted from [Sanguesa et al., 2021]. 5

1.2 The operating pressure, temperature, and CO_2 concentration for different CCUS technology. 8

2.1 Atmospheric gases and their respective freezing temperature gases from [NOAA, 2023] https://www.noaa.gov/jetstream/atmosphere 24

3.1 Characteristics of Zeolite 13X used in this study. 45

4.1 Comparison of total work, by percentage, required to run the system with precompression and turbine recovery (TR, Figure 3.1c) compared to the no compression system (NC, Figure 3.1a) at T_1 = -20 °C for n = 400, 800, and 2000. A positive percentage means that TR takes more work than the corresponding NC case, and a negative percentage means TR takes less work than the corresponding NC case 65

4.2 Percent differences in work required to run the system between TR (Figure 3.1c) and no precooler (ε = 0) and NC (Figure 3.1a) with a precooler (ε = 0.7) for various compression ratios and inlet temperatures. 66

4.3 Adsorption isotherm constants for Zeolite 13X at -50°C 66

List of Figures

Page

Figure

1.1 A visual representation of the Carbon Cycle, referenced from [NOAA, 2019] 1

1.2 GHG emisisons in 2020 from the US. CO_2 emissions are the largest contributor of total GHGs. [EPA, 2022] 3

1.3 Radiative forcing of GHGs over time. CO_2 contributes the most to the total radiative forcing of all GHGs, and has steadily increased since the 1950's. 3

1.4 The annual CO_2 emissions from fossil fuel and industry over time, and global CO_2 concentration in the atmosphere. Emissions and overall concentration have steadily increased since the 1950's. 6

1.5 Renewable energy generation by technology from 2010 to 2021 and evaluated for 2030 sustainability goals. Data adapted from [IEA, 2022b] 6

1.6 Four subcategories of DAC systems, pre-combustion, oxy-combustion, post-combustion, and direct air capture. 8

1.7 Proposed DAC systems evaluated in the present study to determine energy consumption. 11

2.1 Overview on sorbent materials used in carbon capture. 18

2.2 Liquid DAC systems use absorption to capture gas molecules and solid DAC systems use adsorption to capture gas molecules. 19

2.3 Specific SA is a crucial characteristic of sorbent material for CO_2 capture. In the figure, it is shown that a more porous material will have a higher specific SA. 21

2.4 Sorbents investigated in [Kumar et al., 2015]. 23

2.5 Sorbents investigated in [Madden et al., 2017]. 23

2.6 The absolute humidity of air at various temperatures. As temperature decreases, the humidity amount in the air tends towards zero. One can assume the humidity is negligble in ultra-low temperatures. 27
2.7 The PSA cycle steps. 29
2.8 An overview on 2-bed 4-step Skarstrom cycle. The columns are synchronized with an 180-phase shift in steps such that one column is adsorbing and the alternate column is desorbing at any given time. 30
2.9 Schematic of the gas separation unit, modified from [Wilcox, 2012]. 33
3.1 Proposed systems to evaluate the possible energy benefit of precompression of atmospheric air for a cryogenic CO_2 capture system. 37
3.2 Proposed systems to evaluate the possible energy benefit of a PSA unit in a cryogenic CO_2 capture system. 44
3.3 A model of the PSA system. A compressor is used to fill a chamber with air to the adsorption pressure. 45
3.4 A simple adsorption model of a pure substance. 50
3.5 ELI Adsorption model of a mixture with 2 adsorbate species. 51
4.1 Temperature required to desublimate mass fraction ω of CO_2 for various compression ratios 55
4.2 Total work required for the no compression case (NC) (Figure 3.1a) to desublimate CO_2 at various inlet temperatures with a precooler effectivess of $\varepsilon = 0.7$ 56
4.3 Factor increase of work required for both the PC and TR cases, compared to the baseline NC case, all utilizing a precooler with $\varepsilon = 0.7$ and ambient temperatures of (a) -20 °C, (b) -40 °C, and (c) -65 °C. For each value of ω, from left to right, the first set of bars represents $n = 400$, the second set of bars represents $n = 800$, and the third set of bars represents $n = 2000$. . . 59

4.4 Total work required to run PSA versus NC at various mass fractions at a heat exchanger effectiveness $\varepsilon = 0.7$. 62
4.5 Work input to the cryocooler as the inlet CO_2 concentration is varied. 63
4.6 Work of the cryocooler (red) and work of the PSA unit (blue) at $\varepsilon = 0.7$. . . 64

Chapter I

Introduction

Significance of the Study

All living things are made of carbon, as carbon is an essential building block of all organic matter. Carbon is continuously cycling through our entire ecosystem [Dey et al., 2022], as seen through the Carbon Cycle in Figure 1.1. The Carbon Cycle elucidates the fluctuations of carbon throughout the atmosphere, ocean, and lithosphere between carbon sources and carbon sinks. A source is described as an activity or process that emits carbon dioxide (CO_2) into the atmosphere. Sources can be anthropogenic, such as power plants [Nassar et al., 2017], or natural, such as volcanoes [Plank and Manning, 2019]. Carbon sinks absorb and store CO_2. Carbon sinks can also be anthropogenic, such as afforrestation [Humpenöder et al., 2014], or natural, such as the ocean [Quéré et al., 2016].

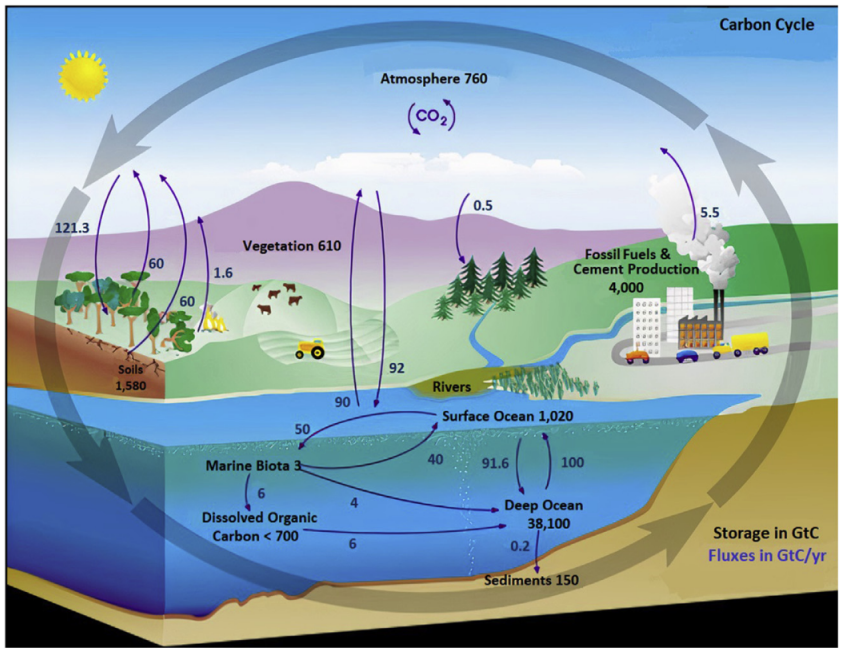

Figure 1.1: A visual representation of the Carbon Cycle, referenced from [NOAA, 2019]

In the Pre-Industrial Era (1750 and earlier), carbon sources and carbon sinks counteracted one another and stabilized the CO_2 concentration to approximately 280 ppm [Stein, 2022]. However, in the past two centuries, human activities have increased emissions at a rate quicker than carbon sinks can handle. Activities like agriculture, industry, waste disposal, deforestation, and fossil fuel consumption produce copious amounts of greenhouse gases (GHG) into the atmosphere [Wuebbles and Jain, 2001]. GHGs are gases in the Earth's atmosphere with the ability to trap solar infrared radiation and re-emit back to Earth, raising the planet's temperature through a greenhouse effect. Some greenhouse gases (GHGs) include carbon dioxide (CO_2), methane (CH_4), nitrous oxide (N_2O), flourinated gases, and water vapor (H_2O). GHGs are crucial for life on Earth, as scientists say the planet's average temperature would be approximately 33°C colder than without the naturally occurring greenhouse effect [NAP, 1992]. However, anthropogenic GHG emissions, not natural, are the area concern. Anthropogenic activities are estimated to have caused 1°C of global warming since the Pre-Industrial Era [IPCC, 2018].

CO_2 has gained the most traction in terms of climate change above the other GHGs for numerous reasons. Out of all the GHGs, CO_2 is the most abundant, by a significant amount. In 2020, CO_2 was the largest contributor of the total GHG emissions in the US for that year, almost 80% (Figure 1.2). In comparison to other GHGs, it is difficult to quantify the lifetime of CO_2 in the atmosphere due to the varying timescale of the CO_2 processes in the Carbon Cycle. However, the Intergovernmental Panel on Climate Change (IPCC), an intergovernmental body under the United Nations created to assess science related to climate change and provide policymakers at all levels of government with knowledge, recommendations, and potential risks associated with climate change, estimates 15-40% of CO_2 emissions until 2100 will remain in the atmosphere for more than 1000 years. [IPCC, 2014b]. CO_2 has the highest positive radiative forcing (RF) [IPCC, 2014a] of all GHGs. RF is a measure of how much a climate driver contributes to climate change. RF is the energy difference per area of a driver entering and leaving the atmosphere. A positive

RF indicates a ”warming effect” such that the energy entering the atmosphere is more than the energy leaving the atmosphere. As seen in Figure 1.3, CO_2 has the highest positive RF, and the rate of increase in total RF of GHGs is surpassed by CO_2. CO_2 emissions from anthropogenic activities is the largest driver of climate change [Forster et al., 2007].

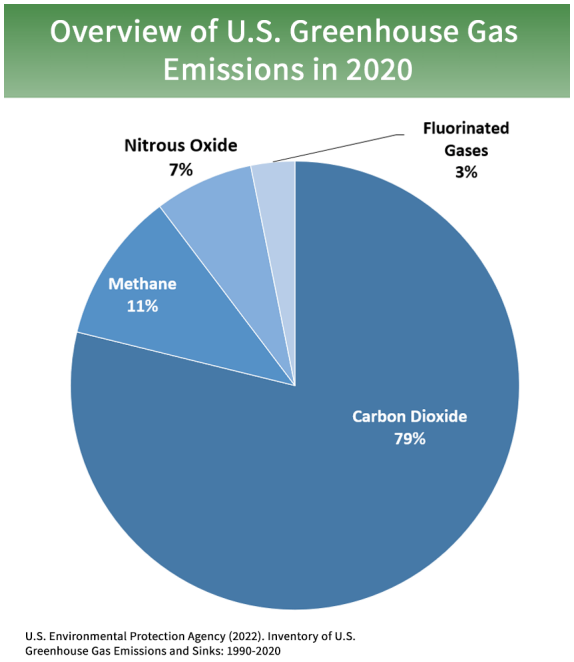

Figure 1.2: GHG emisisons in 2020 from the US. CO_2 emissions are the largest contributor of total GHGs. [EPA, 2022]

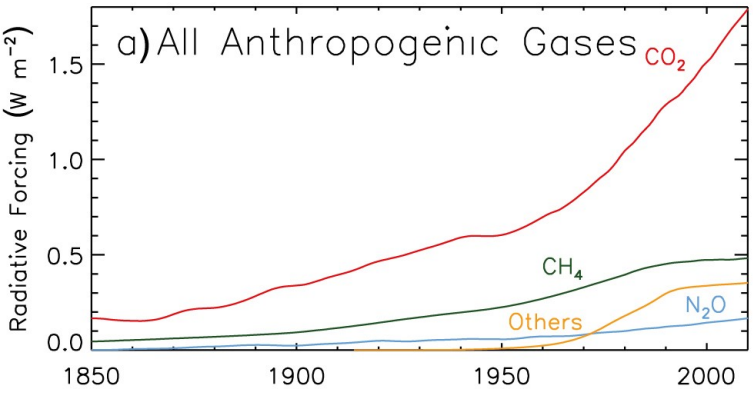

Figure 1.3: Radiative forcing of GHGs over time. CO_2 contributes the most to the total radiative forcing of all GHGs, and has steadily increased since the 1950’s.

The conference of parties (COP) is an international global climate summit held annually by the UN to evaluate the current status of and reach an international agreement to combat climate change. COP21 in 2015, or better known as the Paris Climate Conference that produced the Paris Agreement, was the first time ever an international agreement was globally accepted to recognize and combat climate change. The Paris Agreement is intended to limit global warming to below 2°C, preferably under 1.5°C [UN, 2015]. United Nations (UN) Secretary General Antonio Guterres expressed his concern and urgency for action against climate change at the conclusion of COP27 in November 2022, "Climate chaos is a crisis of biblical proportions. The signs are everywhere. Instead of a burning bush, we face a burning planet." [UN, 2022]

Efforts have been and are currently underway to decrease CO_2 emissions, a process called decarbonization. Decarbonization can happen in many sectors: transportation, energy generation and consumption, the built environment, agriculture, and land use. In the energy generation sector, switching to low-carbon energy generation methods will lower CO_2 emissions. Countries around the world are implementing renewable energy grids. Iceland, Norway, Costa Rica, Brazil, and Canada generate more than 60 percent of their energy through hydropower [Kroposki et al., 2017]. Solar photovolatic (PV) energy generation increased 22% from 2020 to 2021 worldwide, with the US generating almost 150,000 GWh of energy through solar in 2021 [IEA, 2022c], [IEA, 2023]. In the transportation sector, switching to electric vehicles (EVs) over conventional internal combustion engine vehicles decreases GHG emissions [EPA, 2023]. Around the world, the EV market share has steadily increased from 2013, as seen in Figure 1.1 [Sanguesa et al., 2021]. In the built environment, new policies are enforced to lower the global warming potential of refrigerants in HVAC systems [Voigt, 2021] and increase energy efficiency in newly constructed buildings [Commission, 2022]. In agriculture and land use, promoting sustainable farming practices such as regenerative agriculture to improve soil health can improve the Carbon Cycle to draw CO_2 from the atmosphere [Rhodes, 2017].

Table 1.1: EV Market share as a percentage of total vehicle sales in that country per year from 2013-2020. Most countries have seen an increase in EV sales over time. Data adapted from [Sanguesa et al., 2021].

Country	2013	2014	2015	2016	2017	2018	2019	2020
Norway	6.10	13.84	22.29	27.40	29.00	39.20	49.10	55.90
Iceland	0.94	2.71	3.98	6.28	8.70	19.00	22.60	45.00
Sweden	0.71	1.53	2.52	3.20	3.40	6.30	11.40	32.20
The Netherlands	5.55	3.87	9.74	6.70	2.60	5.40	14.90	24.60
China	0.08	0.23	0.84	1.31	2.10	4.20	4.90	5.40
Canada	0.18	0.28	0.35	0.58	0.92	2.16	3.00	3.30
France	0.83	0.70	1.19	1.45	1.98	2.11	2.80	11.20
Denmark	0.29	0.88	2.29	0.63	0.40	2.00	4.20	16.40
USA	0.62	0.75	0.66	0.90	1.16	1.93	2.00	1.90
United Kingdom	0.16	0.59	1.07	1.25	1.40	1.90	22.60	45.00
Japan	0.91	1.06	0.68	0.59	1.10	1.00	0.90	0.77

Nonetheless, we are not decarbonizing fast enough. Although renewable energy generation reached record highs, in order to meet a Net Zero Emissions target by the IEA, renewable energy generation must be near 23,000 TWh by 2030, while renewable energy was near 8,000 TWh in 2021. As seen in Figure 1.5, the rate of growth for renewable energy production is not increasing fast enough to meet emission targets. On a global scale, CO_2 emissions from fossil fuels and industry are not decreasing. In fact, annual CO_2 emissions increased over 50% from 2010 to 2021 (see Figure 1.4), [Ritchie et al., 2020]. In order to meet the goal of limiting Earth's temperature increase to 1.5°C (the Paris Agreement threshold), global anthropogenic CO_2 emissions must decline from 45 percent of 2010 levels by 2030 [IPCC, 2018].

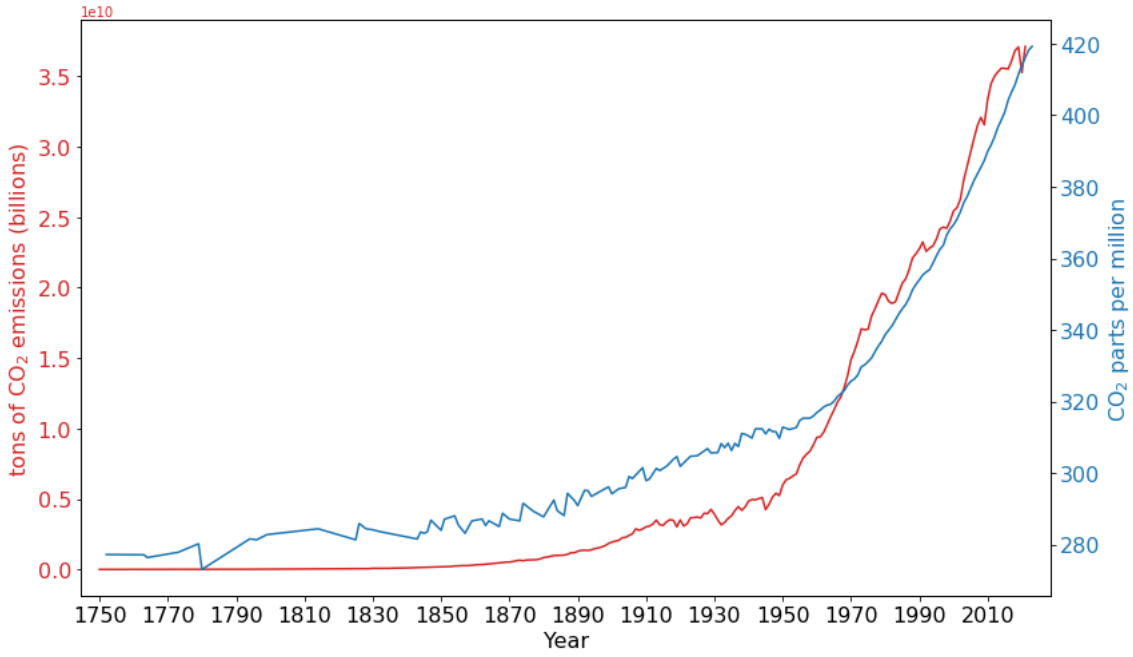

Figure 1.4: The annual CO_2 emissions from fossil fuel and industry over time, and global CO_2 concentration in the atmosphere. Emissions and overall concentration have steadily increased since the 1950's.

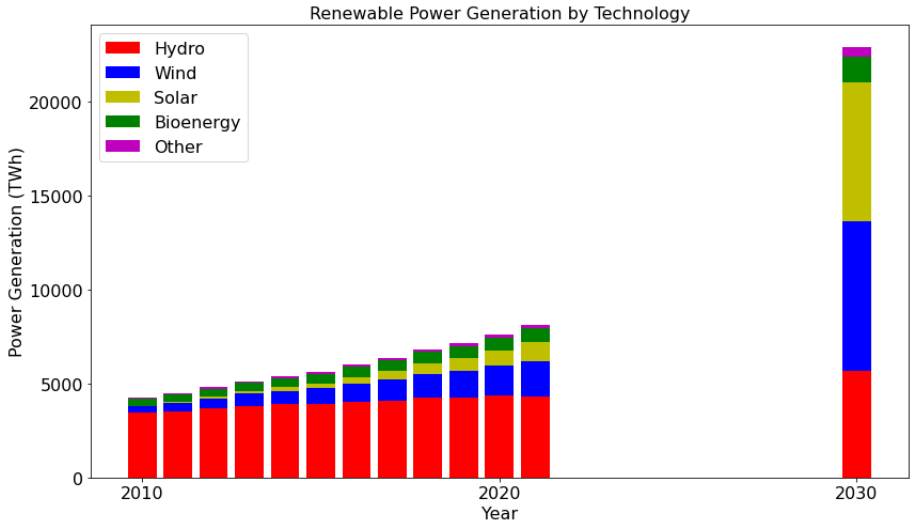

Figure 1.5: Renewable energy generation by technology from 2010 to 2021 and evaluated for 2030 sustainability goals. Data adapted from [IEA, 2022b]

To make the situation more egregious, there are some sectors where decarbonization is difficult. A 2014 study discussed the feasibility of decarbonizing industries where decreasing CO_2 emissions will be a challenge [Davis et al., 2018]. These industries include transportation (aviation, shipping, long-distance road), material production (iron, steel, cement), and load-following electricity. In 2021, these "hard-to-eliminate' CO_2 emissions accounted for almost 30 percent of the share of global GHG emissions [Ritchie et al., 2020]. In the a special IPCC report, it is stated "The deployment of carbon dioxide removal (CDR) to counterbalance hard-to-abate residual emissions is unavoidable if net zero CO_2 or GHG emissions are to be achieved." [IPCC, 2022]

Decarbonization will not solely solve climate change. A multi-prong approach utilizing different practices such as carbon removal technologies, decarbonization, and carbon emissions reductions must be used in conjunction to slow down and eventually reverse global warming. Carbon removal technologies, also known as carbon dioxide removal (CDR) or negative emission technologies (NET), cover a wide variety of approaches to decrease CO_2 emissions from the atmosphere. Some of these approaches include carbon capture with utilization and storage (CCUS), afforestation, or bioenergy with carbon capture and sequestration [Press, 2019].

CCUS is the process that captures CO_2 emissions from sources such as coal-fired power plants or ambient air environments, and reuses or stores it so it will not enter the atmosphere. CCUS encompasses 4 technologies: pre-combustion, oxy-combustion, post-combustion, and direct air capture. Figure 1.6 and Table 1.2 reflect the mechanisms and operating conditions for each technology [Lai et al., 2021].

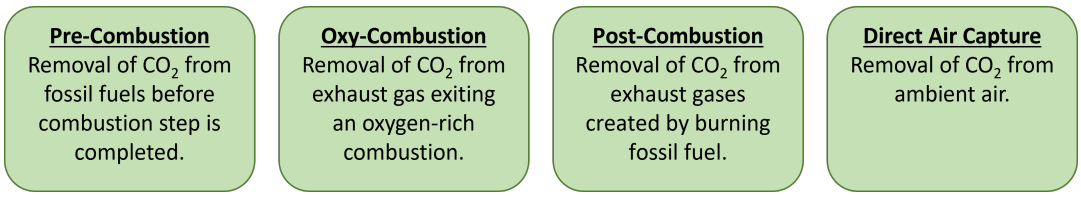

Figure 1.6: Four subcategories of DAC systems, pre-combustion, oxy-combustion, post-combustion, and direct air capture.

Table 1.2: The operating pressure, temperature, and CO_2 concentration for different CCUS technology.

CCUS Technology	**Pressure (bar)**	**Temperature (°C)**	**CO_2 Concentration (%)**
Pre-combustion	14-70	200-450	15-60
Oxy-combustion	1	-55	17-70
Post-combustion	1	40-60	3-20
Direct Air Capture	1	25	0.04

Pre-combustion carbon capture removes CO_2 from the fossil fuel before combustion occurs. This method uses a controlled gasification process to produce synthesis gas (or syngas) to be used for power generation. This approach is advantageous because the CO_2 concentration is relatively high, between 15% – 60% [Sanz-Perez et al., 2016]. Due to the high concentrations of CO_2 in the gas stream, pre-combustion carbon capture can be more efficient than other CCUS, however there are high capital costs are associated with gasification process meaning other technologies are more cost-effective [DoE, 2022]. R&D is directed towards improving the gasification stage, advanced turbine systems for increased efficiency, and sorbent material to lower costs.

Oxy-combustion carbon capture is the process of combustion using an oxygen-rich inlet gas stream, yielding exhaust gas comprised of mainly of CO_2 and H_2O. The concentration

of CO_2 in the exhaust gas stream is very high, up to 70%, and the CO_2 can be captured by condensing the water in the exhaust stream. Oxy-combustion requires large amounts of oxygen in the system compared to the other CCUS technology, increasing overall costs. Oxy-combustion is advantageous because of the limited NOx emissions due the removal of nitrogen in a preliminary step, high CO_2 concentrations in the exhaust stream, and the applicability to existing power plants [DoE, 2022].

Post-combustion carbon capture separates CO_2 from flue gas streams. The concentration of CO_2 in exhaust gas is between 3% – 20%. Due to low concentration of CO_2 and low operating pressure of the exhaust stream, this method requires larger volumes of air to be processed, overall increasing energy requirements and costs. As most anthropogenic CO_2 emissions come from stationary sources with combustion systems, such as coal or gas power plants, post-combustion capture is advantageous because it can be retrofitted to existing power plants to capture carbon at the source [Metz et al., 2005]. Amine scrubbing is a well-established and currently deployed post-combustion CC technology, utilizing amine-based solutions to absorb CO2 from exhaust gas [Rochelle, 2009].

Direct Air Capture (DAC) carbon capture is the process of removing CO_2 from ambient air conditions. Compared to the other CCUS technology, a major disadvantage of DAC is the low CO_2 concentration in ambient air conditions, approximately 0.04%. However, DAC is advantageous because it does not require to be placed in a specific location (i.e., point source carbon capture). Pre-combustion, oxy-combustion, and post-combustion CO2 capture requires system placement near a powerplant or CO_2 source. Costs associated with transporting the captured carbon to storage facilities can be avoided.

While some of the NETs are commissioned today, the scale at which these technologies are deployed will not make a crucial impact to mitigate climate change [Sovacool et al., 2022]. In contrast to other CDRs, DAC has the potential to be scaled up to remove large amounts of CO_2 [Press, 2019]. Additionally, other NETs face significant barriers for upscaling, such

as land use, economic and social viability.

Statement of the Problem

There are 18 pilot DAC plants operating around the world capturing 0.01MtCO_2 per year, however DAC must be scaled up to 60 MtCO_2 per year by 2030 to meet target goals [IEA, 2022a]. DAC technology is still in its infancy and requires more research and development into evaluating the performance of large scale plants in order to meet targets for mitigating climate change [Sovacool et al., 2022]. Recommended research includes system modeling for large scale carbon capture to determine energy consumption [Press, 2019].

Purpose Statement

The purpose of this thesis is to model the energy consumption of novel DAC systems for large-scale use. These systems utilize a combination of DAC techniques to minimize energy consumption. The systems to be evaluated are shown in Figure 1.7. This thesis will answer the following questions

1. What are the mechanisms for direct air systems?
2. What is the energy consumption analysis for DAC?
3. How can DAC processes combine to increase the efficiency of carbon capture?

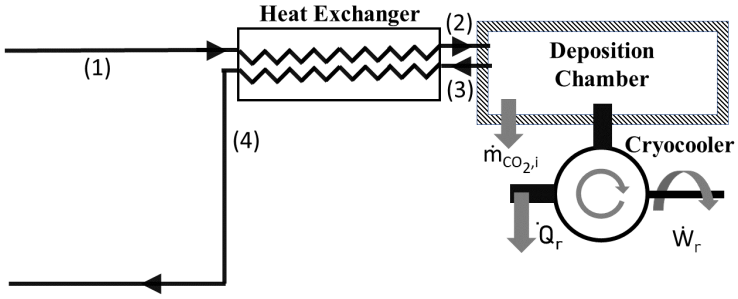

(a) NC (no compression)

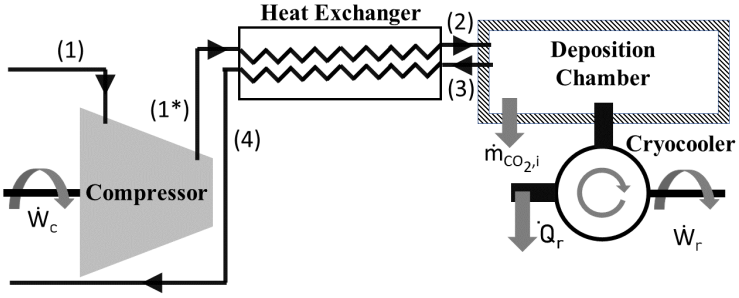

(b) PC (precompression)

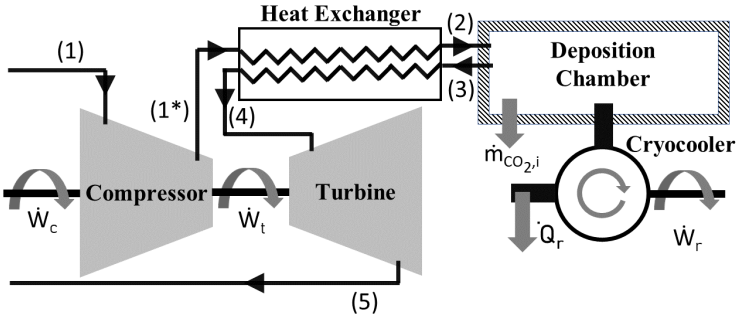

(c) TR (Turbine Recovery)

Figure 1.7: Proposed DAC systems evaluated in the present study to determine energy consumption.

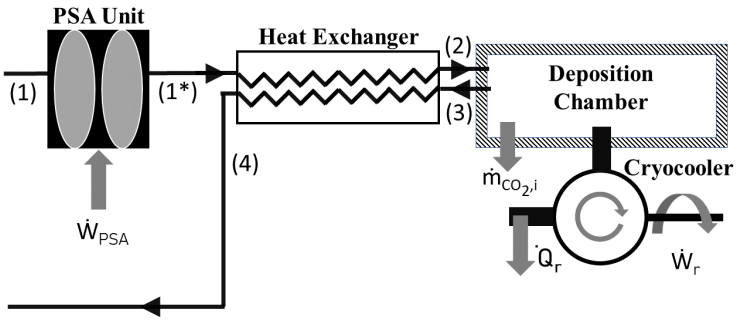

(d) PSA (pressure swing adsorption)

Figure 1.7: Proposed DAC systems evaluated in the present study to determine energy consumption (cont.)

Scope of Study

The scope of this research is atmospheric cryogenic CO_2 capture. Modifications are made to the cryogenic system to improve energy performance of the system. In Chapter 2, background is given on DAC, cryogenic systems, PSA systems, and sorbent material atmospheric carbon capture. Chapter 3 is the energy analysis of the systems in Figure 1.7. Chapter 4 discusses the results from the system model calculations from Chapter 3. Chapter 5 will conclude the research and summarize the major findings.

Limitations

Assumptions are made to simplify the system model. A major assumption is assuming the fluid stream behaves as an ideal gas. A gas behaves as an ideal gas when the compressibility factor Z is equal to 1. This occurs when the state pressure is small relative to the critical pressure and/or the state temperature is large relative to the critical temperature.

The mass flow rate of air entering and leaving the system is constant. Fluid properties

are considered constant at each state. Precompression of low temperature atmospheric air is assumed to be isothermal. The turbine is assumed to be adiabatic and isentropic. The heat exchanger is also assumed adiabatic. For PSA, there is no heat transfer between the gas molecules and the sorbent material. The rate of adsorption and desorption is in equilibrium. No axial mass or thermal dispersion is considered in this study.

Variables

c_v	specific heat at constant volume
d_p	diameter of sorbent particle
H	total enthalpy
H_{air}	total enthalpy of air
H_{CO_2}	total enthalpy of CO_2
$h_{CO_2,desub}$	specific enthalpy of desublimated saturated CO_2
h_{ig}	specific latent heat of sublimation
h_x	specific enthalpy at state x
K	equilibrium constant k_a/k_d
k_a	adsorption rate constant
k_d	desorption rate constant
m_{air}	mass of air
$\dot{m}_{air,x}$	mass flow rate of air at state x
m_{CO_2}	mass of CO_2
$\dot{m}_{CO_2,desub}$	mass flow rate of desublimated CO_2
$\dot{m}_{CO_2,x}$	mass flow rate of CO_2 at state x
n	compression ratio
$P*_x$	compression pressure
P_{ads}	adsorption pressure
P_i	partial pressure of the adsorbate component i

P_{total}	adsorption pressure plus pressure drop across the chamber
$P_{vap,x}$	vapor pressure at T_x
P_x	pressure at state x
q_i	amount of adsorbed component i per unit mass of adsorbent
$q_{max,i}$	maximum amount of adsorbate component i the adsorbent can hold
$\dot{Q}_r$	heat transfer rate required to desublimate ω
R	universal gas constant
s_x	specific entropy at state x
T_{ads}	adsorption temperature
T_C	temperature of the cold environment
T_{desub}	desublimation temperature
T_H	temperature of the hot environment
T_x	temperature at state x
u	specific internal energy
u_s	superficial fluid velocity x
v_{ads}	specific volume at adsorption step
$\dot{W}_c$	work of the compressor
$\dot{W}_{in}$	total net work to run DAC system
$\dot{W}_{PSA}$	work of the compressor
$\dot{W}_r$	work of the cryocooler
$\dot{W}_t$	energy recovery from the turbine
y_i	mole fraction of component i
Z	compressibility factor

Greek Letters

β	coefficient of performace (COP) for a reverse-Brayton cryocooler

β_{Carnot}	carnot COP
γ	specific heat ratio c_p/c_v
ε	void fraction of the PSA chamber
ε_{HX}	heat exchanger effectiveness
ζ_{ads}	rate of adsorption
ζ_{des}	rate of desorption
η	second law efficiency
θ	fraction of the sorbent surface covered in sorbate
θ_v	fraction of the sorbent surface vacant and available for adsorption
ϕ	spherecity of the sorbent particles
ω	mass fraction of desublimated CO_2

Definition of Terms

adsorption	adhesion of molecules to a surface
cryogenic distillation	gas separation technique via the difference of component boiling points in a gas mixture
adsorbate	molecules of species that adhere to surface
adsorbent	surface in which molecules adhere to
fouling	accumulation of solid in the heat exchanger due to low temperatures

List of Acronyms

CC	carbon capture
CO_2	carbon dioxide
DAC	direct air capture
GHG	greenhouse gas

H_2O	water/water vapor
HVAC	heating, ventiliation, and air-conditioning
HFC	hydrofluorocarbons
IPCC	intergovermental pannel of climate change
IEA	international energy agency
CH_4	methane
N_2O	nitrous oxide
NC	no compression
PPM	parts per million
PFC	perflurocarbons
PC	precompression
PSA	pressure swing adsorption
RF	radiative forcing
TR	turbine recovery

Chapter II

Literature Review

Anthropogenic atmospheric CO_2 plays the largest role among greenhouse gasses in modifying Earth's climate [Strassmann et al., 2008], and several research groups are working on CO_2 removal from energy production and industrial-process flue gas as well as directly from the air. The major capture processes include adsorption, absorption, membrane separation, and cryogenic capture [Aaron and Tsouris, 2005], [Choi et al., 2011].

DAC has been used for other purposes besides climate change mitigation such as spacecraft life support [Sherif and Knox, 2005] or on submarines. DAC was first introduced to the scientific community as a CO_2 mitigation strategy in 1999 by Lackner [Lackner et al., 1999]. Lackner evaluated the thermodynamic feasibility of collecting CO_2 using $Ca(OH)_2$ (calcium hydroxide) in a liquid solvent system. Lackner argued that although the CO_2 concentration in ambient air conditions is low, it is not too low for DAC to be unachievable.

The first step of DAC is to intake large quantities of air to be put in contact with an agent or environment that will remove the CO_2 from the gas stream. The CO_2 is sequestered and concentrated from the air. The agent is then recycled through a state-altering process that regenerates the material for continued use. If the air it to be in contact with an environment for carbon capture, the environment is held to a state where CO_2 removal occurs. The final step of DAC is the transportation of CO_2 to a long-term storage site [Sovacool et al., 2022]. The scope of this research does not include the transportation step in DAC. The following sections will review materials used to capture carbon, and will provide an in-depth overview on cryogenic distillation and pressure swing adsorption for DAC.

Sorbent Material for DAC

This section will discuss sorbent material used for DAC systems. Commonly used

CO_2 adsorbents can be classified into the follow groups: aqueous (liquid) solvents, solid sorbents, membranes, and resins as seen in Figure 2.1.

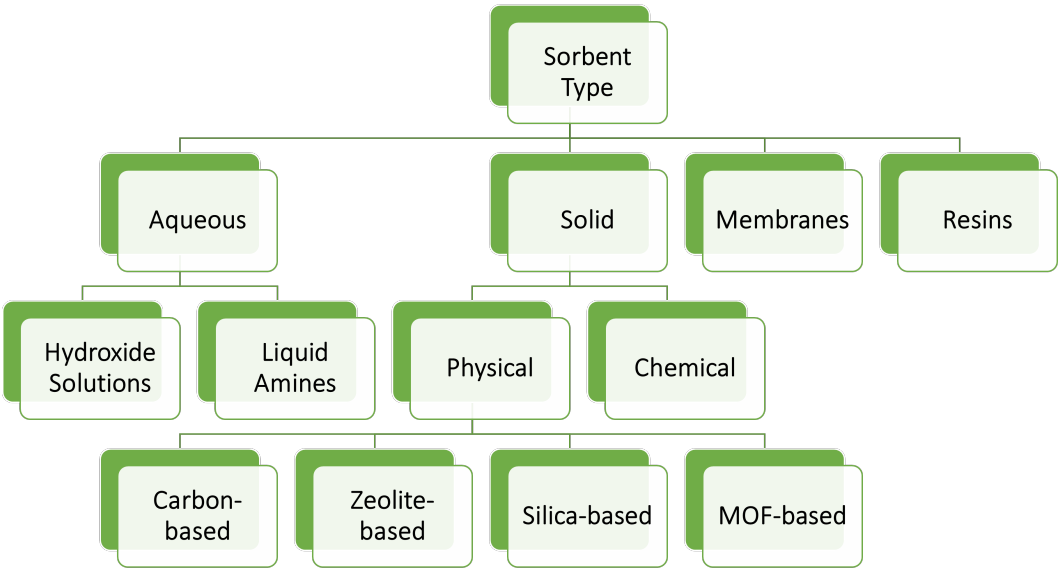

Figure 2.1: Overview on sorbent materials used in carbon capture.

In liquid DAC systems, gas molecules concentrate in the solvent medium through a mechanism called absorption. In contrast for solid DAC systems, the gas molecules concentrate to the surface of the sorbent through a process called adsorption. Figure 2.2 visually represents the difference between absorption and adsorption for carbon capture.

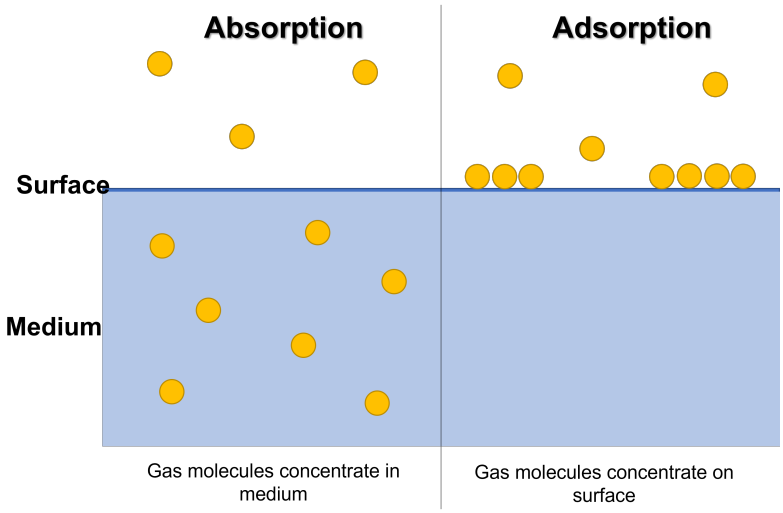

Figure 2.2: Liquid DAC systems use absorption to capture gas molecules and solid DAC systems use adsorption to capture gas molecules.

Aqueous solvents use a strong basic hydroxide solution to capture CO_2. The CO_2 molecules react with ions in the solution to produce a carbonate precipitate. The solvent has a high CO_2 capacity and uptake, however the precipitate by-product requires high temperatures to later release the CO_2. Liquid amines are also commonly used for post-combustion capture, also known as amine scrubbing. Liquid amines have high CO_2 adsorption capacity, but they are corrosive to system equipment and can have harmful effects on the local environment [Leonzio et al., 2022].

Solid sorbents encompass a wide variety of materials. Firstly, they can be characterized through the bond strength to the CO_2 molecule, also called the heat of adsorption [McQueen et al., 2021]. Physical adsorption through weak intramolecular forces, or physisorption, occurs when the heat of adsorption is less than 15 kcal/mol = 63 kJ/mol. Chemical adsorption through strong covalent bonds, or chemisorption, occurs when the heat of adsorption is greater than 15 kcal/mol = 63 kJ/mol. Solid sorbents are comprised of various precursors and can be modified for desired characterizes. Sorbents can be carbon-

based, non-carbon based, or amine-functionalized. Solid sorbents are porous materials and are also organized based on the pore size [Abd et al., 2020]. The International Union of Pure and Applied Chemistry classifies pore size as

1. Micropores: ≤ 2 nm
2. Mesopores: 2-50 nm
3. Macropores: ≥ 50 nm

Resins are another category of sorbent material that have recently been researched and developed for direct air carbon capture [Wang et al., 2020]. Ion exchange resins utilize the moisture swing adsorption mechanism, or a humidity swing, to capture and release CO_2. Resins can be modification with amine functional groups to affect surface properties and capture performance. Resins have a lower energy adsorption and desorption requirement compared to liquid or solid sorbents; however, it is not as technologically mature.

Desired Sorbent Characteristics.

There are many properties of sorbents that must be evaluated to determine applicability for DAC. The sorbent material should meet certain criteria for both economical and operational requirements. When examining sorbent criteria, ideal sorbents should have high CO_2 adsorption rate and capacity, high selectivity, easy regeneration with cyclic performance, cost-effective operation, high availability, and stability (chemically, thermally, structurally). The adsorption capacity or loading is the amount of adsorbate taken up by the adsorbent per unit mass (or volume) of the adsorbent [Abd et al., 2020]. Selectivity of a sorbent is the ratio of CO_2 capacity to another gas capacity [Abd et al., 2020]. Sorbents for carbon capture should have a high adsorption capacity and high selectivity for CO_2.

Specific surface area is another key criteria for selecting a sorbent material. The specific surface area is the surface area (SA) per unit mass. A material that is more porous has an

increased specific surface area. Figure 2.3 demonstrates that a more porous material has a higher specific SA. In Figure 2.3, there is a uniform cube with length of each side of 10 m. The SA of the cube is equal to the area of a side a cube multiplied by 6 sides (600 m^2). The specific SA is equal to the total SA divided by the mass of the cube, so the specific SA is 6 m^2/g. In the bottom of Figure 2.3 , the same cube is now divided in half in each direction to expose a new surface. The lengths of the side of each cube are 5 m and now there are 8 cubes. The specific SA of this new configuration is 12 m^2/g. A material having a greater pore structure and distribution will also have a larger specific SA. Modifications to increase a sorbent material specific SA will increase its performance for carbon capture.

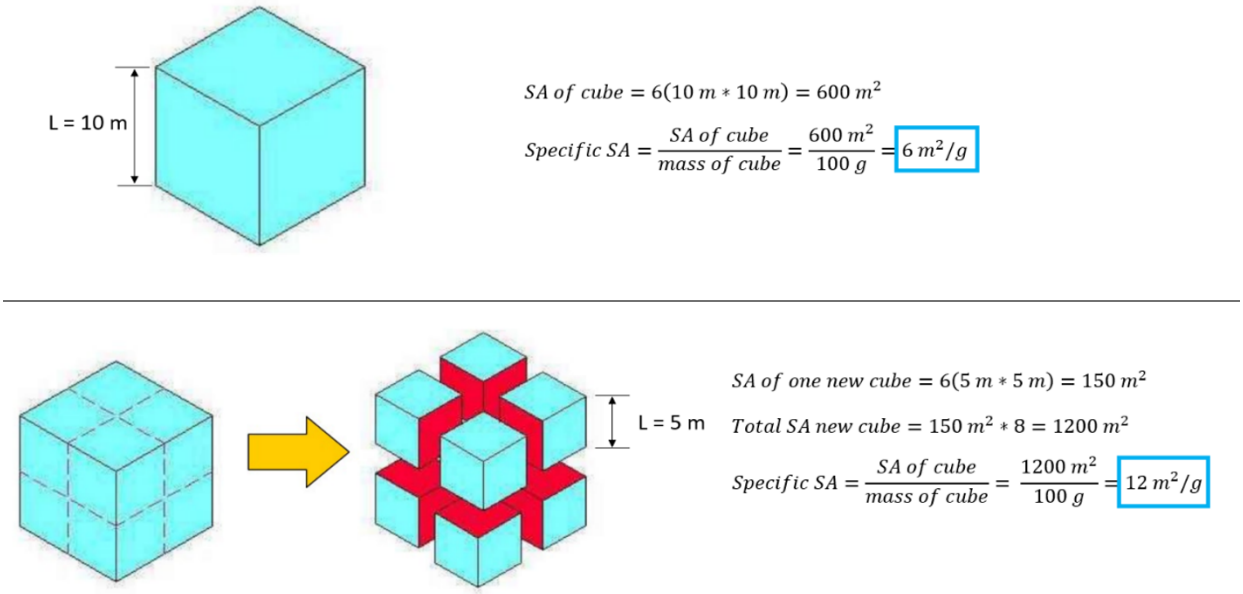

Figure 2.3: Specific SA is a crucial characteristic of sorbent material for CO_2 capture. In the figure, it is shown that a more porous material will have a higher specific SA.

Well Performing Sorbents for DAC.

As mentioned previously, physical adsorption interactions between CO_2 molecules and the sorbent surface are governed through weak intramolecular forces. These forces are

highly dependent on the surface area of the sorbent material [Oschatz and Antonietti, 2018]. Thus, materials with larger surface areas are desirable for DAC. Solid sorbent materials that are currently employed or being researched for DAC carbon capture are activated carbon (AC), metal organic frameworks (MOFs), zeolites, silica gels, and carbon nanotubes [Ozkan and and, 2022], [Liu et al., 2021]. Carbon-based materials have good structural stability and resistance to moisture, but surface inertness make them ineffective in low CO_2 concentration [Hao et al., 2011]. Zeolite-based materials have high selectivity for CO_2 in dilute gas streams but are prone the water degradation. Silica-based materials require surface modification to be used for carbon capture [Lai et al., 2021]. Metal organic frameworks (MOFs) also have a high affinity for CO_2 in diulte concentrations, but are sensitive to water as well.[Gargiulo et al., 2020], [Hu et al., 2018].

[Kumar et al., 2015] evaluated how water vapor affects the performance of 5 sorbent materials for DAC: one chemisorbent TEPA-SBA15 (mesoporous silica) and four physisorbents Zeolite 13X (zeolite), HKUST-1 (MOFs), Mg-MOF-74/Mg-dobdc (MOFs), SIFSIX-3-Ni (hybrid material). Temperature-programmed desorption (TPD) experiments were ran on the sorbents. TPD is used to indicate the water vapor affinity and required regeneration energy of the sorbent material. The results from the TPD experiments show that chemisorbent TEPA-SBA-15 performed better than the physisorbents in terms of water affinity. Zeolite 13X performed the worst of the physisorbents. Stability tests were also performed on the sorbents at 40C and 75% humidity to represent their shelf life over 1,7, and 14 days. Zeolite 13X performed the best of the physisorbents in the stability tests. Although zeolites exhibit a high affinity for H_2O [Shi et al., 2022], this is not an issue in ultra low temperature environments where humidity levels are negligible. This is discussed further in Chapter 3.

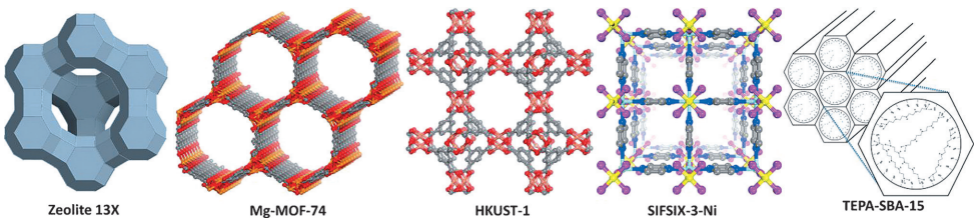

Figure 2.4: Sorbents investigated in [Kumar et al., 2015].

[Madden et al., 2017] extended the experiments of [Kumar et al., 2015] to 10 other physisorbents: 4 hybrid ultramicroporous materials (HUMs) SIFSIX-3-Cu, SIFSIX-2-Cu-i, DICRO-3-Ni-i and MOOFOUR-1-Ni, 5 prototype MOFs ZIF-8, DMOF-1, UiO-66, UiO-66-NH2 and MIL-101, and 1 ultra microporous metal-organic material (MOM) Ni-4-PyC. These sorbents were tested similarly as in the previous study to determine simulated DAC performance and the affect of water vapor on performance. SIFSIX-3-Cu performed the best in DAC environments, however it also performed the worst in stability tests. The study found that physisorbents have a lower regeneration energy than chemisorbents, which may offset the poor performance in some categories.

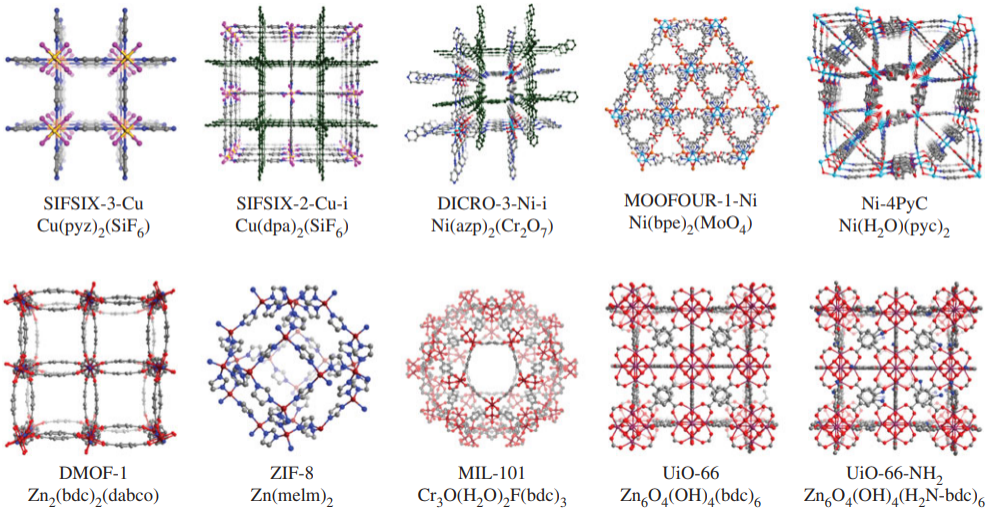

Figure 2.5: Sorbents investigated in [Madden et al., 2017].

[Bao et al., 2022] evaluated the performance of Zeolite 13X for CO_2 enrichment to achieve an increased target concentration at the exit stream. An enrichment factor, defined as the ratio of exit CO_2 concentration to inlet CO_2 concentration peaked at 9, indicating an increase from 400ppm to 3600ppm. The enrichment factor is also called concentration factor in literature [Wilcox et al., 2017]. Additionally, cyclic tests determined good cyclic stability of Zeolite 13X after 20 cycles. Overall, Zeolite 13X is a promising sorbent for DAC.

Cryogenic Arctic/Antartic DAC

Cryogenic DAC capitalizes on CO_2 possessing the highest phase-transition temperature of the atmospheric gases (see Table 2.1), except for water vapor (which is easy to eliminate via desiccant wheel or cooling, either due to low ambient temperatures or by conventional refrigeration).

Table 2.1: Atmospheric gases and their respective freezing temperature gases from [NOAA, 2023] https://www.noaa.gov/jetstream/atmosphere

Gas		Freezing Temperature (K)	Concentration in Air
Nitrogen	N_2	63	78.084%
Oxygen	O_2	54.36	20.947%
Argon	Ar	73.85	0.934%
Carbon dioxide	CO_2	194.65	0.035%
Neon	Ne	27.102	18.182 parts per million
Helium	He	0.95	5.24 parts per million
Methane	CH_4	91.15	1.70 parts per million
Krypton	Kr	115.75	1.14 parts per million
Hydrogen	H_2	13.95	0.53 parts per million
Nitrous oxide	N_2O	182.29	0.31 parts per million
Carbon monoxide	CO	68.15	0.10 parts per million
Xenon	Xe	161.35	0.09 parts per million
Ozone	O_3	80.95	0.07 parts per million

At first glance, this approach appears to be thermodynamically favorable because the entropy absorbed for CO_2 desublimation is the quotient of thermal power transferred from

the gas to the cryocooler divided by the temperature at which the heat lift occurs ($\dot{Q}/T$). Since $\dot{Q}$ is fixed by the CO_2 latent heat of sublimation, the magnitude of entropy lift is reduced by increasing the desublimation temperature, T. Reduced cold-end entropy absorption induces corresponding reduction in cryocooler input power. Despite the apparent benefit and near-universal use of compression to that point, Yuan et al. [Yuan et al., 2014] challenged the need for compression. They found that for typical flue-gas CO_2 concentrations, compression always consumes more power than the associated power reduction obtained by increasing the desublimation refrigeration temperature. Even with generous energy recovery by running the compressed gas through a turbine after CO_2 extraction, compression still carries an energy penalty.

Yuan et al. [Yuan et al., 2014] found that the compression energy penalty decreases with decreasing CO_2 partial pressure. However, they only examined flue gas and did not extend their study to direct-air cryogenic CO_2 capture where the CO_2 partial pressure is much lower than power plant effluent. Typically, for power plant flue gases, the concentration of CO_2 is as high as 13-15% versus the amount of CO_2 in the atmosphere, which is around 0.04% (or 400 ppm). Caustic gases, such as sulfur dioxide, are also found in flue gas and need to be handled during the CO_2 desublimation process; whereas for direct-air capture (DAC) in cold climates, the need to remove other components, such as water vapor, is minimal. Furthermore, flue gas temperatures are on the order of 150°C versus below zero for DAC systems placed in arctic climates. Depending upon system design, volumetric flow rates may also be orders of magnitude less for flue gas than for DAC.

Many articles have explored flue-gas cryogenic CO_2 separation using a variety of thermodynamic processes, all of which involve an initial compression step. Among reported flue-gas CO_2 separation techniques where effluent is compressed, there are three main subsets: 1) Reverse-Brayton-like processes that recover some power while achieving low temperature by expanding CO_2-laden gas through a turbine [Baxter et al., 2009, Burt et al., 2009,

Zanganeh et al., 2009]; 2) Joule-Thompson-like processes that achieve low temperature by throttling CO_2-laden gas with no turbine power recovery [Li et al., 2016]; and 3) processes that do not treat CO_2-laden gas as the principal working fluid and achieve low temperature by removing heat from the gas via an external cryocooler [Schach et al., 2011, Song et al., 2012, Xu et al., 2012, Swanson et al., 2012].

While several research groups mention the flue gas compression energy penalty to concentrate CO_2 prior to deposition, Yuan et al. [Yuan et al., 2014] were the first to formally investigate whether increased compression power to achieve decreased refrigeration power carried a net energy penalty. They found increasing flue gas pressure with no turbine energy recovery suffers energy penalties that increase with compression ratio. Surprisingly, even with generous turbine energy recovery, there remains an energy penalty for flue gas compression. In short, it *always* takes more power to compress than the associated power reduction obtained through desublimation refrigeration temperature for CO_2 concentrations in flue gas.

Cryogenic distillation is a promising approach to DAC because it 1) produces pure CO_2 in solid, liquid, or gas form that carries economic value and/or can be easily stored; 2) does not rely on development of new or experimental materials; and 3) is amenable to rapid scale-up to industrial production whereas the other techniques are not [Font-Palma et al., 2021]

Agee et al. [Agee et al., 2013] first described a DAC cryogenic CO_2 system scaled for global atmospheric CO_2 reduction with numerous stations sited across Antarctica. For average global atmospheric CO_2 partial pressure of 3.9 x 10^{-4} atm and average Antarctic ambient temperature of 226 K (-47.15 °C), the CO_2 desublimation temperature is 133 K (-140.15 °C). By placing the DAC system in Antarctica, the energy required to reduce the air temperature down to 133 K (-140.15 °C) from ambient, is significantly reduced compared to being in a location where the ambient air temperature averages around 25 °C). Another advantage of placing the DAC system in an arctic climate is that at very low temperatures,

water is largely absent from the atmospheric air. According to Fig. 2.6, which represents the maximum possible amount of moisture in the air at a particular temperature, the amount of water the air can contain exponentially decreases as the air temperature becomes colder. A follow-on representative benchtop experiment used a liquid-nitrogen-cooled apparatus to reduce CO_2 content of entrapped air. CO_2 reduction from 443.71 ppm to 50.17 ppm (89% depletion) was demonstrated after 325 minutes by cooling to 129 K (-144.15 °C). CO_2 reduction from 485 ppm to 35.8 ppm (93% depletion) was achieved after 333 minutes by cooling to 125 K (-148.15 °C) [Agee and Orton, 2016]. Subsequent analysis by the present authors [von Hippel, 2018, **?**] extended the research by quantifying energy requirements and scaling issues for such a system. The purpose of the current work is to examine compression of atmospheric air for cryogenic CO_2 capture to determine whether this unexplored low-CO_2 partial-pressure region of compression yields a net energy benefit.

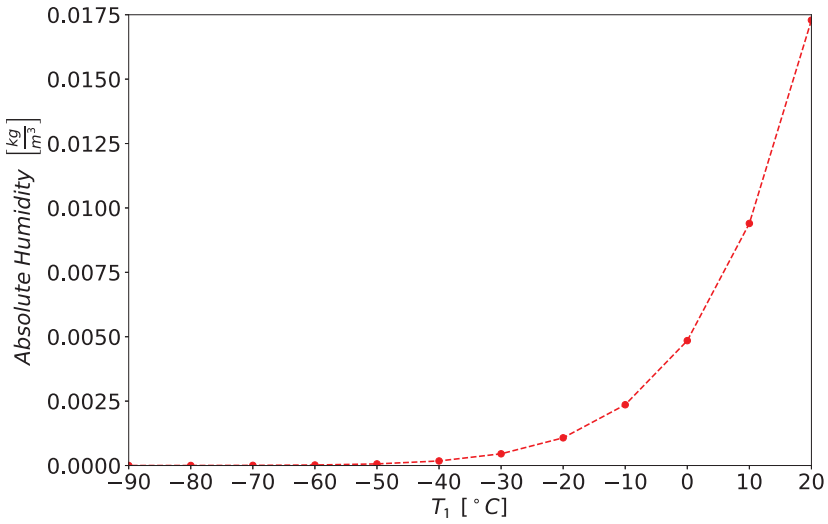

Figure 2.6: The absolute humidity of air at various temperatures. As temperature decreases, the humidity amount in the air tends towards zero. One can assume the humidity is negligble in ultra-low temperatures.

Pressure Swing Adsorption DAC

DAC systems can function using a sorption-based approach for carbon capture. In the adsorption process, gas molecules of a component (the adsorbate) concentrate at the surface of a solid, (adsorbent/sorbent) due to intramolecular forces between the fluid and solid [Agarwal, 2010]. The adsorption processes are cyclic and "swing" between two steps, adsorption and desorption, and allows the adsorbent material to be regenerated for continued use. There are 2 main sorption techniques for CO_2 capture: Pressure Swing Adsorption (PSA) and Temperature Swing Adsorption (TSA). PSA utilizes pressure differentials to capture CO_2 and regenerate the sorbent. A compressor or pump is used to raise the pressure of the fluid to P_{ads}. At high pressures, the fluid molecules have affinity to the adsorbent surface. The pressure of the fluid is decreased to P_{des} to regenerate the sorbent. Vacuum swing adsorption (VSA) is a modification of PSA technology used for carbon capture where P_{des} is less than P_{atm}. TSA alternates the temperature of the sorbent to adsorb and desorb for CO_2 capture and sorbent regeneration. Other less mature adsorption techniques are Moisture Swing Adsorption (MSA) and Electric Swing Adsorption (ESA). MSA uses the evaporation of water as the driving force for CO_2 adsorption [Sun et al., 2021]. ESA is variation of TSA where the heat is generated in situ passing an electric current through a conductor [Ribeiro et al., 2014]. Adsorption approaches may be combined, such as TVSA (Temperature Vacuum Swing Adsorption) or PVSA (Pressure Vaccum Swing Adsorption).

Pressure swing adsorption is an established technology used in many industrial applications. First patented by Charles W. Skarstrom in the 1960s [Skarstrom, 1958], PSA can be used for hydrogen purification, air separation, noble gas purification, CO_2 capture, and other applications [Grande, 2012]. Adsorption is acclaimed for DAC due to its high efficiency in separating dilute mixtures [McQueen et al., 2021]. The Skarstrom Cycle involves a 2-bed, 4-step process demonstrated in Figure 2.8. PSA is a batch process, however by commissioning the adsorption/desorption step correctly, a continuous flow can be achieved

[Tien, 2019]. The steps of the cycle are:

1. Pressurization: Valve is closed, air flows to increase P to P_H
2. Feed: Adsorption occurs at P_H
3. Blowdown: Valve is opened, P in chamber decreases to P_L
4. Purge: Desorption occurs at P_L. Air at P_L flows through the chamber to flush out the adsorbate species

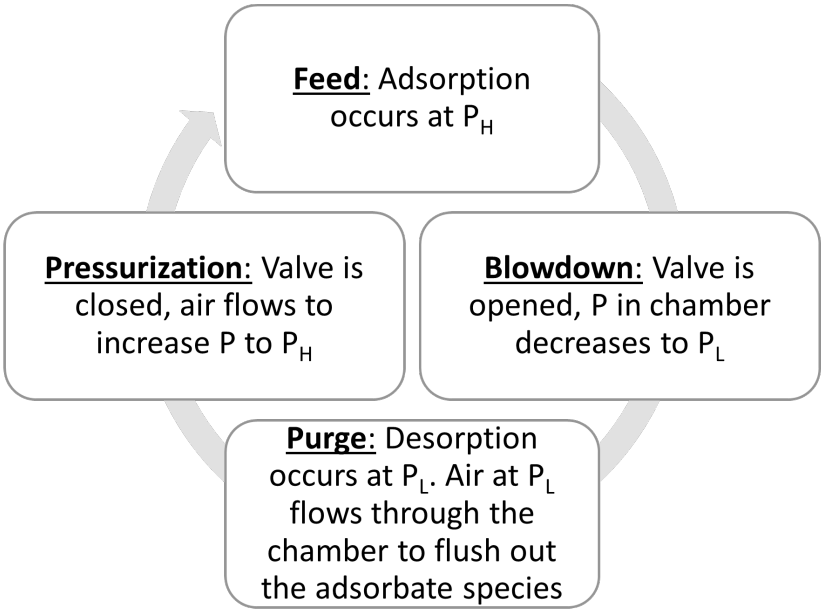

Figure 2.7: The PSA cycle steps.

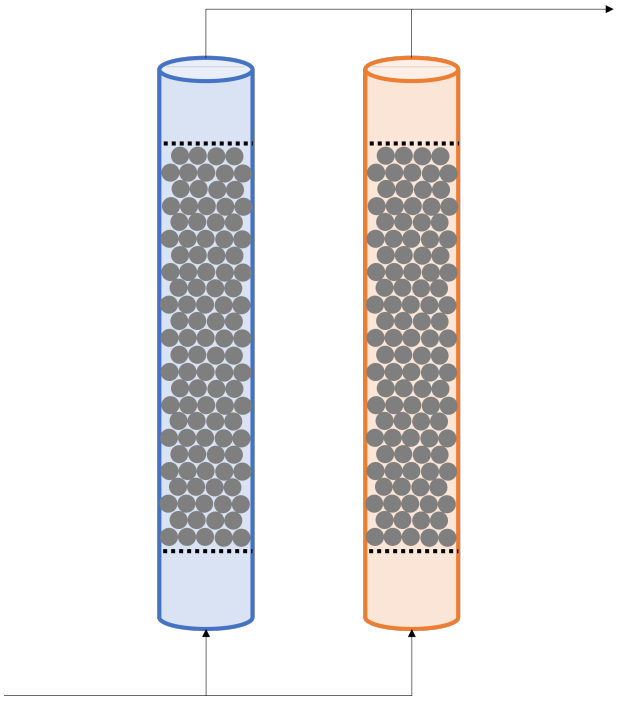

(a) Example column setup for a Skartstrom cycle

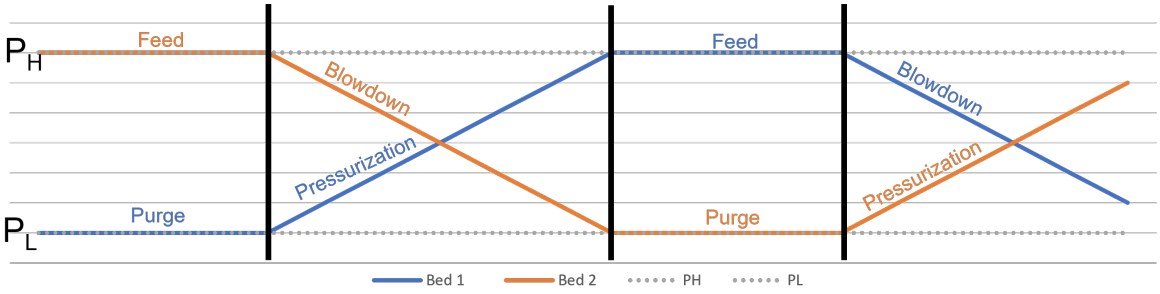

(b) Pressure of the column at each step in the cycle

Figure 2.8: An overview on 2-bed 4-step Skarstrom cycle. The columns are synchronized with an 180-phase shift in steps such that one column is adsorbing and the alternate column is desorbing at any given time.

[Shendalman and Mitchell, 1972] first modeled the Skastrom PSA cycle in 1972. They experimentally evaluated the separation process of He-CO_2 using silica gel as the sorbent material. In parallel, they derived an analytical solution for an ideal model assuming He as

an inert gas with no co-adsorption effects, equilibrium between the rate of adsorption and desorption at all times, and the adsorption model follows a linear isotherm. The pressurization and blowdown steps are assumed instantaneous. [Chan et al., 1981] extended the analysis of Shendalman and developed an equilibrium theory model for a feed mixture of 2 components, A and B, to determine cycle performance characteristics. They assumed linear isotherms, negligible dispersion axially or radially, and negligible pressure drop. The system model operates at steady state operation. The Chan model matches the Shendalman model when component B is assumed to be inert and no adsorption effects occur.

[Chue et al., 1995] compared the performance of activated carbon (AC) and Zeolite 13X on CO_2 capture from flue gas using PSA. First, they experimentally measured pure CO_2 and N_2 adsorption isotherms, and fitted the data using Langmuir Isotherms. Next, they measured the equilibrium selectivity (selectivity of CO_2 over N_2) for a binary mixture and fitted the data using the Extended Langmuir Isotherms. In both cases, Zeolite 13X was a better sorbent than AC. According to the mathematical model results, Zeolite 13X had a more favorable PSA performance over a wide range of cycle parameters than AC. Adsorption for bulk separation is better with Zeolite 13X than AC. Concurrently, Chue solved a mathematical model of a non-isothermal, adiabatic 3-bed, 7-step PSA process to compare cycle performance of the two materials to determine the better performing sorbent. In all cases, Zeolite 13X was superior.

Few models of adsorption processes for DAC systems on a holistic approach are found in literature. [Zhao et al., 2019] thermodynamically modeled a TVSA cycle to capture CO_2 from indoor environment at concentrations of 400 ppm, 700 ppm, 1000 ppm, 2000 ppm and 3000 ppm. Zhao et al approximated the work input for the vacuum as

$$W_{pump} = \frac{1}{\eta_{pump}} RT_{des} ln\left(\frac{P_{ads}}{P_{des}}\right) \tag{II.1}$$

where W_{pump} is the work of the pump, η_{pump} is the efficiency of the pump, T_{des} is the desorption temperature and P_{ads} and P_{des} are the adsorption and desorption pressures, respectively.

[Sabatino et al., 2021] developed an analysis of a VTSA process and determined the work of the pump as

$$W_{pump} = \frac{1}{\eta_{pump}} \dot{m} c_p T \left(\frac{p_{out}}{p_{in}}^{\frac{\gamma-1}{\gamma}} - 1 \right) \tag{II.2}$$

where is the mass flow rate of the air, c_p is the specific heat at constant pressure, p_{in} and p_{out} are the pressure of the fluid stream entering and leaving the pump, respectively. γ is defined as $\frac{c_p}{c_p - R}$.

[Liu et al., 2022] modeled the energy consumption of a VPSA cycle as

$$EC_{ads} = \frac{1}{\eta_c y_{CO_2}} RT_{ads} ln \left(\frac{P_{ads}}{P_{atm}} \right) \tag{II.3}$$

$$EC_{des} = \frac{1}{\eta_v} RT_{ads} ln \left(\frac{P_{atm}}{P_{des}} \right) \tag{II.4}$$

where η_c and η_v is the efficiency of the compressor and pump, respectively, set to 0.7; y_{CO_2} is the concentration of CO_2 in the inlet stream.

[Wurzbacher et al., 2016] developed a transient mass and heat transfer model of the desorption step of VTSA process with an amine-based sorbent APDES-NFC-FD. The model is used to evaluate the recovered gas stream during desorption and the describe the purity level of CO_2 at this step, a kep performance indicator for large scale DAC. The study key findings for VTSA systems are: fast diffusion in the vacuum step indicate a uniform gas

phase composition in the sorbent material, and a reference point for geometric dimensions of a desorption chamber in a VTSA system.

Various literature pieces introduce the theory of minimum separation work, or the free energy of mixing, to determine the energy consumption of carbon capture systems. [Lackner et al., 1999] noted majority of the energy consumption for a DAC system comes from regenerating the sorbent. To regenerate the sorbent, energy must be added to the system to overcome the binding energy of CO_2 to the sorbent. The binding energy is equal to the free energy of mixing, G, is given as

$$\Delta G = RT\,log\frac{P}{P_0} \tag{II.5}$$

where P is the regeneration pressure and P_0 is ambient pressure. The free energy required to separate CO_2 from ambient air is 20 KJ/mol. The theoretical energy is independent of separation technique. However, inefficiencies in sequestration processes can quickly accumulate and inflate the system energy consumption. Other works agreed the theoretical minimum energy consumption of carbon capture system can be explained through free energy of mixing [House et al., 2009, Wilcox, 2012, Lackner, 2013, Zhao et al., 2017, Gür, 2022]. The process is visualized in Figure 2.9

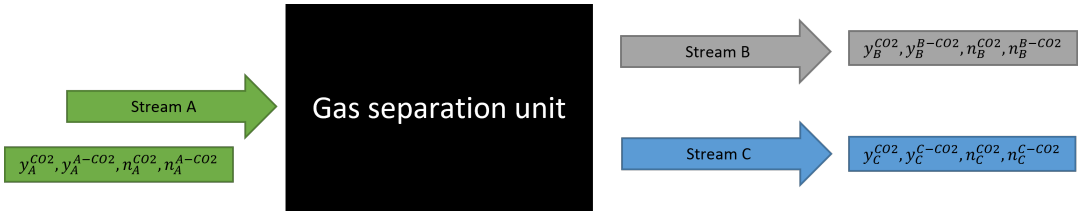

Figure 2.9: Schematic of the gas separation unit, modified from [Wilcox, 2012].

A version of Equation II.5 is shown below in Equation II.6

$$
\begin{aligned}
W_{min} = RT[n_B^{CO_2} ln(y_B^{CO_2}) + n_B^{B-CO_2} ln(y_B^{B-CO_2})] \\
+ RT[n_C^{CO_2} ln(y_C^{CO_2}) + n_C^{C-CO_2} ln(y_C^{C-CO_2})] \\
- RT[n_A^{CO_2} ln(y_A^{CO_2}) + n_A^{A-CO_2} ln(y_A^{A-CO_2})]
\end{aligned} \tag{II.6}
$$

where $n_B^{CO_2}$ is the number of CO_2 moles in steam B, $y_B^{CO_2}$ is the mole fraction of CO_2 in stream B, $n_B^{B-CO_2}$ is the number of moles of all gases but CO_2 in Stream B, and $y_B^{B-CO_2}$ is the mole fraction of all gases but CO_2 in Stream B. The rest of the variables follow the same nomenclature for Stream A and C.

The actual energy consumption of a DAC system can be calculated using second law efficiency [Lively and Realff, 2016]. The second law efficiency accounts for losses in system processes, described in Equation II.7

$$
\eta = \frac{W_{min}}{W_{actual}} \tag{II.7}
$$

where η is the second law efficiency, W_{min} is the minimum energy, and W_{actual} is the actual energy consumption of the system.

[Ruthven, 2014] argued the free energy of mixing does not sufficiently reflect the energy consumption for separating dilute concentrations CO_2 from air. Ruthven introduces the idea of the value function. Ruthven calculates the energy cost of DAC is 650 KJ/mol, 2 orders of magnitude greater than the minimum separation work.

Chapter III

Methodology

Energy Analysis: Precompression of Atmospheric Air

System Model Overview. A thermodynamic analysis was performed on a cryogenic refrigeration cycle to calculate the ideal compressor energy depletion in precompression (PC) and the turbine energy recovery output described in TR. The total work required to desublimate CO_2 is determined utilizing a novel approach adopted from psychrometrics. Psychrometrics is the thermodynamics of gas-vapor mixtures, typically applied to air-water mixtures in heating, ventilating, and air-conditioning (HVAC) analysis. For this cryogenic application, the mixture comprises air and CO_2. Other components will not be considered as CO_2 has the highest freezing temperature in atmopsheric gases (see Table 2.1. The thermodynamic model, based on psychrometric principles, was adapted from [Boetcher et al., 2019] to analyze the air-CO_2 mixture. The system schematics are shown in Figure 3.1.

In Figure 3.1b, atmospheric air enters the compressor (State 1) and is compressed to a compression factor before entering the heat exchanger (State 1*). The compressed airstream is precooled via the heat exchanger (State 2) and enters the deposition chamber to desublimate the CO_2. The cold, high pressure, CO_2-lean airstream exits the deposition chamber (State 3), passes through the HX to precondition the incoming airstream, and then exits the system (State 4). As discussed previously, increasing the partial pressure of CO_2 increases the desublimation temperature. In Figure 3.1c, a similar system is used however a turbine is utilized (State 5) to recover energy from the high pressure, CO_2-lean airstream exiting the system.

Figure 3.1a represents the baseline system model to compare the techniques to. No precompression of atmospheric air is used. In the present study, thermodynamic modeling,

based on psychrometric principles, is applied to a theoretical DAC system to gain insight on the energy requirement of precompression (PC) and turbine recovery (TR) systems. The theoretical system is situated in a low-temperature Arctic/Antarctic environment, where the ambient temperature or effective ambient temperature that takes into account night sky radiative cooling varies between -20 °C and -90 °C and operates at a current-technology-level feasible compression (which includes compression ratios up to 2000).

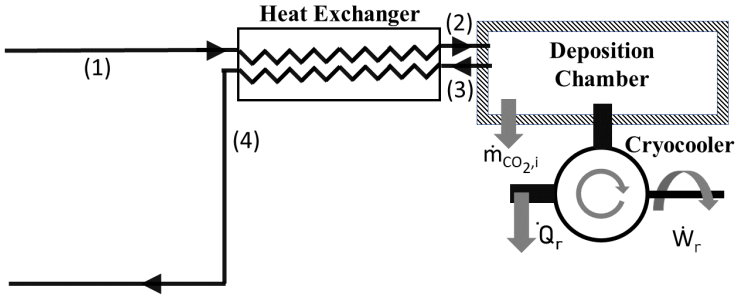

(a) NC (no compression)

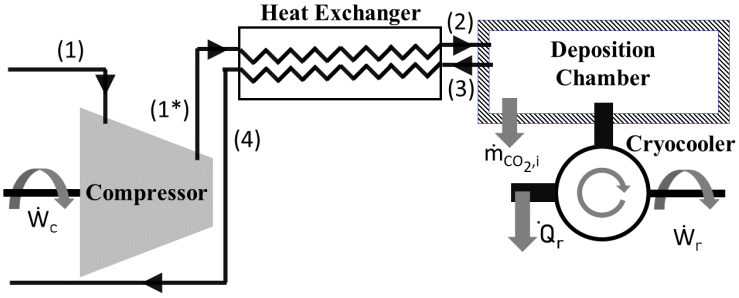

(b) PC (precompression)

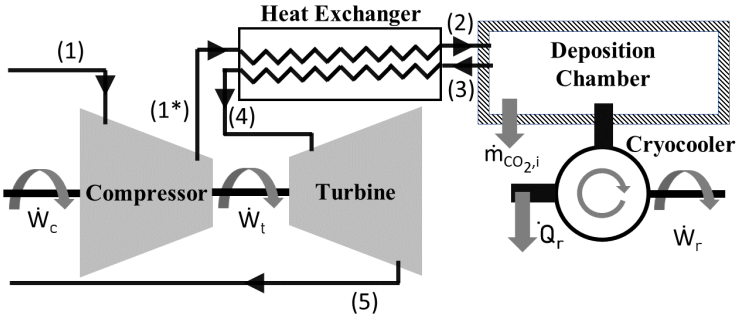

(c) TR (Turbine Recovery)

Figure 3.1: Proposed systems to evaluate the possible energy benefit of precompression of atmospheric air for a cryogenic CO_2 capture system.

The total enthalpy, H, for the studied mixture is defined as

$$H = H_{air} + H_{CO_2} = m_{air}h_{air} + m_{CO_2}h_{CO_2} \tag{III.1}$$

In this equation, H_{air} and H_{CO_2} are the total enthalpies of the air and CO_2, respectively, in the mixture, and h_{air} and h_{CO_2} are the corresponding specific enthalpies. The masses of air and CO_2 in the mixture are m_{air} and m_{CO_2}. The following expression defines the specific enthalpy of the air-CO_2 mixture

$$h \equiv \frac{H}{m_{air}} = h_{air} + \frac{m_{CO_2}}{m_{air}}h_{CO_2} \tag{III.2}$$

According to conservation of mass, the mass of the air flowing through the systems in Figure 3.1 is constant and equal to $\dot{m}_{air}$. The conservation of mass equation for the CO_2 in the deposition chamber is

$$\dot{m}_{CO_{2,2}} = \dot{m}_{CO_2,i} + \dot{m}_{CO_{2,3}} \tag{III.3}$$

Here, $\dot{m}_{CO_{2,2}}$ and $\dot{m}_{CO_{2,3}}$ are the mass flow rates of the CO_2 at states 2 and 3, respectively. The mass of CO_2 desublimated, $\dot{m}_{CO_2,i}$, which is assumed to be a saturated solid, is determined by a targeted, specified mass fraction to be desublimated (for further explanation see the Results and Discussion section) defined as

$$\omega = \frac{\dot{m}_{CO_2,i}}{\dot{m}_{CO_2,2}} \tag{III.4}$$

The mass of the CO_2 prior to the deposition chamber is constant; likewise, the mass of the CO_2 after the deposition chamber also remains constant.

Compressor and Recovery Turbine.

The atmospheric air, at pressure P_1, enters the compressor and is isothermally compressed to a pressure, P_{1^*}. The amount of compression is specified by the compression ratio, n.

$$n = \frac{P_{1^*}}{P_1} \tag{III.5}$$

The assumption of isothermal compression is a bounding idealization. Under non-isothermal compression, the fluid is heated significantly, thus partially defeating the purpose of building the DAC system in an arctic climate. It is understood that in order to obtain isothermal compression, the process is slow and an infinite amount of intercoolers are required. Isothermal compression represents the minimum additional energy-cost baseline, that is, if there is not a net benefit without considering the thermodynamics and energy cost of the intercoolers, then considering them in the analysis is a moot point. Further discussion can be seen in the Results and Discussion section. The work of the compressor, when the process is internally reversible, is defined as

$$\frac{\dot{W}_c}{\dot{m}_{air}} = T_1(s_{1^*} - s_1) + (h_1 - h_{1^*}) \tag{III.6}$$

where T_1 (also equal to T_{1^*}) is the ambient temperature, h_{1^*} and h_1 are the specific enthalpies and s_{1^*} and s_1 are the specific entropies of the air-CO_2 mixture before and after the compressor, respectively.

The TR technique includes an additional turbine recovery component that is assumed to be adiabatic and isentropic, another bounding idealization. The energy recovered from the turbine is calculated as

$$\frac{\dot{W}_t}{\dot{m}_{air}} = h_4 - h_5 \tag{III.7}$$

In this equation, h_4 and h_5 are the specific enthalpies of the air-CO_2 mixture before and after the turbine.

Precooling Heat Exchanger. The heat exchanger is implemented to collect the "waste" cooled air leaving the deposition chamber to precool the ambient air entering, thus reducing the heat removal required to cool the deposition chamber to the desublimation temperature. The heat exchanger is assumed to be adiabatic so that all of the heat from the hotter fluid is transferred to the colder fluid. Assuming the capacity rates of both the hot and cold streams are equal, the effectiveness of the heat exchanger is defined as

$$\varepsilon = \frac{T_{1^*} - T_2}{T_{1^*} - T_3} = \frac{T_4 - T_3}{T_{1^*} - T_3} \tag{III.8}$$

Deposition Chamber. The conservation of energy for the deposition chamber is

$$\frac{\dot{Q}_r}{\dot{m}_{air}} = h_3 - h_2 + \frac{\dot{m}_{CO_2,i}}{\dot{m}_{air}} h_{CO_2,i} \tag{III.9}$$

where $\dot{Q}_r$ is the heat transfer rate required to desublimate a mass fraction ω of CO_2. The enthalpies, h_2 and h_3, are the total specific enthalpies of the air-CO_2 mixtures at their respective states. The enthalpy of the desublimated saturated solid CO_2 is $h_{CO_2,i}$.

Cryogenic Refrigeration Cycle.

The coefficient of performance (COP) for the reverse-Brayton cryocooler is defined as

$$\beta = \frac{\dot{Q}_r}{\dot{W}_r} \tag{III.10}$$

where $\dot{W}_r$ is the required work input to the cryocooler. The Carnot COP is the maximum

theoretical COP of a system, which is defined as

$$\beta_{Carnot} = \frac{T_C}{T_H - T_C} \tag{III.11}$$

Here, T_C is the temperature of the cold reservoir or refrigerated space, in this case, T_3, which is set to the desublimation temperature, and T_H is the temperature of the hot environment, which in this case is the ambient temperature, T_1. The second-law efficiency of the system is defined as

$$\eta = \frac{\beta}{\beta_{Carnot}} \tag{III.12}$$

A conservative estimate of the maximum currently attainable second-law efficiency of cryogenic refrigeration systems is around 0.15 [Radebaugh, 2004], which is the efficiency used in the present analysis. However, higher values may be achieved with further research.

Thermal Properties and Analysis.

National Institute of Standards and Technology (NIST) REFPROP 10.0 [Lemmon et al., 2018] was utilized to determine thermodynamic properties of the air and the CO_2 at each state. Properties for air (0.7812 N_2, 0.2096 O_2, and 0.0092 Ar (on molar basis)) are calculated using an equation of state from Lemmon et al. [Lemmon et al., 2000]. Span and Wagner [Span and Wagner, 1996] developed the CO_2 equation of state, which includes the sublimation line.

The National Oceanic and Atmospheric Administration Muana Loa Atmospheric Baseline Observatory measured the atmospheric carbon dioxide concentration at a monthly average of 419 ppm in May 2021 [Muana, 2021]. The value of 419 ppm is directly equal to the mole fraction of CO_2 at the inlet of the DAC system, $x_{CO_2,1}$ = 0.000419. The partial

pressure of the CO_2 can be calculated using the mole fraction

$$P_{CO_2,1} = x_{CO_2,1} P_1 \tag{III.13}$$

The ambient pressure was assumed to be P_1 = 1 atm. Additionally, the pressure for the turbine recovery case (TR) at state 5 was also assumed ambient. The compression ratio, n, was varied incrementally between 1 (no compression) and 2,000. Technically, the partial pressure of the air would be the partial pressure of the CO_2 subtracted from the total pressure. Since the resultant partial pressure of the air was extremely close to the total pressure, for ease of calculations, the partial pressure of the air was assumed to be the total pressure throughout the system (both before and after the desublimation). The DAC system target desublimated mass fraction, ω, of CO_2 was varied between 0.1 and 0.99. The targeted desublimated CO_2 mass fraction was used to calculate the mass fraction of CO_2 remaining in the flow at state 3 ($x_{CO_2,3}$). During the DAC process, the temperature required to desublimate the remaining mass of CO_2 after a portion desublimates continues to decrease. Therefore, the targeted mass fraction at state 3 was used to determine the desublimation temperature, T_3, required to remove the total specified amount of CO_2.

The latent heat of sublimation, h_{ig}, was required to calculate the enthalpy of the desublimated solid, $h_{CO_2,i}$. Since data for the latent heat of sublimation for partial pressures of cryogenic CO_2 is scarce, it was estimated using the Clausius-Clapeyron equation, defined as

$$ln\frac{P_{vap,2}}{P_{vap,1}} = \frac{h_{ig}}{R}\left(\frac{1}{T_1} - \frac{1}{T_2}\right) \tag{III.14}$$

where R is the ideal gas constant, and $P_{vap,1}$ and $P_{vap,2}$ are vapor pressures at temperatures T_1 and T_2 in absolute units.

The ambient inlet temperature at state 1 was varied and set to T_1 = -20 °C, -40 °C, -65 °C, and -90 °C. As explained in von Hippel [von Hippel, 2018] and Boetcher et al. [Boetcher et al., 2019], the first three ambient temperatures are average temperatures of very cold ambient-environment sites: Snag, Yukon, Oymyakon, Russia, and Vostok Station, Antarctica, respectively, and -90 °C is reflective of taking advantage of nighttime radiative cooling at the Vostok site. The effectiveness of the heat exchanger, ε, was varied between 0 (no precooler heat exchanger) and 0.99. Although it is ideal to have a heat exchanger with as high of an effectiveness as possible, several values of ε were tested at the low end to show the relationship between heat exchanger effectiveness and PC and TR.

It was also assumed that the mass flow rate of the air entering and leaving the system is constant and set to $\dot{m}_{air}$ = 1 kg/s. This mass flow rate was selected to put the results on a per-unit-mass-of-air basis. The following equation is used to convert the thermal energy or work required from a per-mass-air basis to per-mass-CO_2 basis.

$$\frac{\dot{Q} \text{ or } \dot{W}}{\dot{m}_{CO_2,i}} = \frac{\dot{Q} \text{ or } \dot{W}}{\dot{m}_{air}} \frac{\dot{m}_{air}}{\dot{m}_{CO_2,i}} \tag{III.15}$$

The total net work required per unit mass CO_2 to run the DAC system is

$$\frac{\dot{W}_{in}}{\dot{m}_{CO_2,i}} = \frac{|\dot{W}_r|}{\dot{m}_{CO_2,i}} + \frac{|\dot{W}_c|}{\dot{m}_{CO_2,i}} - \frac{|\dot{W}_t|}{\dot{m}_{CO_2,i}} \tag{III.16}$$

Energy Analysis: Pressure Swing Adsorption

System Model Overview.

A thermodynamic analysis was performed on the PSA cycle to calculate the energy consumption to run the combined system. The work is calculated with a novel approach using adsorption isotherms and ideal gas assumptions. Figure 3.2 shows the system schematics to be evaluated.

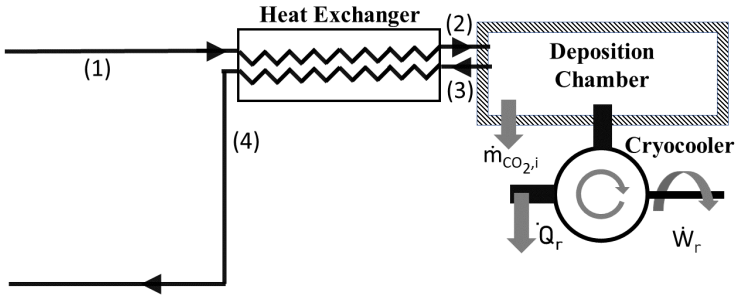

(a) NC (no compression)

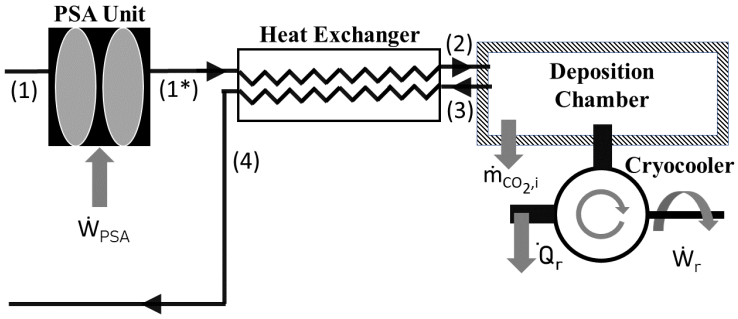

(b) PSA (pressure swing adsorption)

Figure 3.2: Proposed systems to evaluate the possible energy benefit of a PSA unit in a cryogenic CO_2 capture system.

To determine the energy consumption of the PSA unit, $\dot{W}_{PSA}$, the unit can be modeled as seen in Figure 3.3. Atmospheric air is stored in a chamber using a compressor. The chamber is packed with a sorbent material. Zeolite 13X was selected as the sorbent for this system due to its high applicability in PSA systems [Bao et al., 2022]. Sorbent material characteristics and adsorbate chamber paramters are listed in Table 3.1.

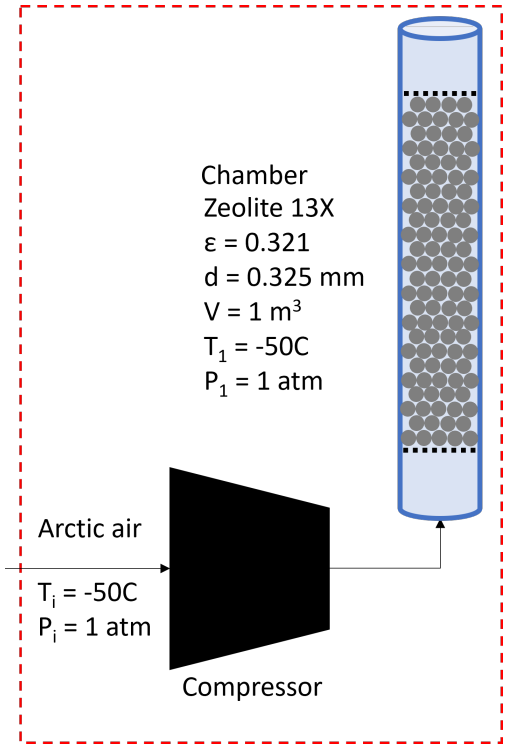

Figure 3.3: A model of the PSA system. A compressor is used to fill a chamber with air to the adsorption pressure.

Table 3.1: Characteristics of Zeolite 13X used in this study.

Zeolite 13X Characteristics		
void fraction	ε	0.321
particle diameter	d_p	0.325 mm
bulk density	ρ	760 kg/m^3

System Model Assumptions.

The assumptions for the model are

1. Chamber with single inlet and no exit
2. Kinetic energy effects and potential energy effects are ignored
3. Tank is filled and emptied rapidly such that Q_{CV} is zero
4. Isentropic relationship such that $Pv^{\gamma} = constant$
5. State of air entering the control volume is constant

Ideal Gas System Model. The gas will be modeled using the ideal gas model. The ideal gas model holds true when the compressibility factor Z is equal to 1. The compressibility factor can be described as

$$Z = \frac{Pv}{RT} \tag{III.17}$$

At states where P is small relative to the critical pressure and T is large compared to the critical temperature, $Z \approx 1$ and the gas behaves as an ideal gas. The ideal gas law is rearranged from Equation III.17 is described as

$$Pv = RT \tag{III.18}$$

where P is the pressure of the gas, v is the specific volume of the gas, R is the universal gas constant, and T is the temperature of the gas. Equation III.18 can be solved to find the specific volume of the gas at state 1, $v_{1,PSA}$.

The PSA processes is assumed to be isentropic with the following relationship

$$Pv^{\gamma} = constant \tag{III.19}$$

where γ is the specific heat ratio. For air, $\gamma = 1.4$. The specific volume of the gas at the adsorption step, v_{ads} can be found using Equation III.19.

Conservation of Energy.

Conservation of energy for a control volume is

$$\frac{dE_{CV}}{dt} = \dot{Q} - \dot{W} + \dot{m}_i(u_i + \frac{V_i^2}{2} + gz_i) - \dot{m}_e(u_e + \frac{V_e^2}{2} + gz_e) \tag{III.20}$$

after applying all assumptions, Equation III.20 reduces to

$$\dot{W} = \dot{m}(du) \tag{III.21}$$

where du is the change in specific internal energy of the air from the desorption step to the adsorption step. Applying the inefficiencies in compressors, the work required of the PSA unit is

$$\dot{W}_{PSA} = \frac{\dot{W}}{\eta_{compressor}} \tag{III.22}$$

$\eta_{compressor}$ was set to 0.7 for this analysis. For a gas mixture following the ideal gas model, u is only a function of temperature. Thus,

$$c_v(T) = \frac{du}{dT} \tag{III.23}$$

where $c_v(T)$ is the specific heat at constant volume of the gas mixture at temperature T. Rearranging Equation III.23 gives

$$du = c_v(T)dT \tag{III.24}$$

The specific heat is found using REFPROP. dT is the change in temperature between the adsorption state and the atmospheric state such that

$$dT = T_{ads} - T_1 \tag{III.25}$$

Pressure Drop in the PSA Chamber.

The chamber is assumed to be fully packed with sorbent material Zeolite 13X, thus the compressor also needs to overcome the pressure drop across the sorbent material. The Kozeny-Carman Equation (Equation III.26) was proposed first by Kozeny in 1927 and later modified in 1925 by Carman. This equation is valid for laminar flow. The pressure drop across the sorbent is independent of the fluid density at low Re flow.

$$\frac{\Delta P}{\Delta L} = \frac{-180\mu}{\Phi^2 d^2}\frac{(1-\varepsilon)^2 u_s}{\varepsilon^3} \tag{III.26}$$

where ΔP is the pressure drop across the sorbent bed, ΔL is the height of the bed, ε is the void fraction of the bed, d_p is the diameter of the sorbent particle, u_s is the superficial fluid velocity, μ is the fluid viscosity and Φ is the sphereicty of the sorbent particles. Φ will be assumed to be 1 for this analysis. The pressure drop found in Equation III.26 is added to the adsorption pressure P_{ads} to find the total pressure needed in the chamber to initiate the adsorption process.

$$P_{total} = \Delta P + P_{ads} \tag{III.27}$$

Adsorption Temperature.

The temperature at the adsorption step, T_{ads} can be calculated rearranging Equation III.18 to

$$T_{ads} = \frac{P_{total} v_{ads}}{R} \tag{III.28}$$

The blowdown step (see Figure 2.7) requires the pressure in the chamber to decrease. Following the ideal gas law, as pressure decreases, the temperature decreases. Thus, the temperature in the chamber will reduce to the inlet temperature T_1 and $T_1 = T_2$.

Adsorption Isotherms.

The Langmuir Isotherm Adsorption models describe the equilibrium adsorption process between the adsorbate species and the adsorbent at constant temperature, as seen in Figure 3.4. The Langmuir Isotherm model is useful to calculate the amount of adsorbed species per unit mass of adsorbent, q. The model is often expressed in terms of θ,

$$\theta = \frac{q}{q_m} \tag{III.29}$$

where θ the fraction of the adsorbent surface covered in the adsorbate and q_m is the maximum amount of adsorbate that the adsorbent can hold.

Some basic assumptions are made to the model:

1. 1 adsorbent molecule per adsorbent site
2. Adsorbed molecules do not interact with one another
3. The adsorbent surface is a uniform surface

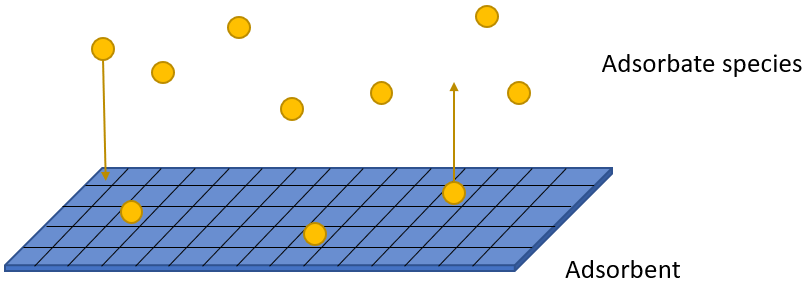

Figure 3.4: A simple adsorption model of a pure substance.

4. Monolayer adsorption

5. The rate of adsorption is equal to the rate of desorption

The rate of adsorption is expressed as

$$\zeta_{ads} = k_a P \theta_v \tag{III.30}$$

where ζ_{ads} is the rate of adsorption, k_a is the adsorption rate constant, P is the pressure of the adsorbate, and θ_v is the fraction of vacant and available. It is also assumed that

$$\theta + \theta_v = 1 \tag{III.31}$$

The rate of desorption is expressed as

$$\zeta_{des} = k_d \theta \tag{III.32}$$

where k_d is the desorption rate constant.

Assuming equilibrium where

$$\zeta_{ads} = \zeta_{des} \tag{III.33}$$

and substituting $K = \frac{k_a}{k_d}$, combining with equation III.31, equation III.33 becomes

$$\theta = \frac{KP}{1+KP} \tag{III.34}$$

K is also known as the equilibrium constant.

The Langmuir Adsorption model assumes a single adsorbate species in the model. However, air is a multi-component mixture and the analysis must reflect the composition of the fluid. The Extended Langmuir Model or ELI is a modification of the Langmuir Adsorption Model to include multiple adsorbate species, as seen in Figure 3.5. Equation III.29 and III.34 are modified to Equations III.35, III.36, III.37, III.38, III.39, III.40, III.41 and III.42 to account for the mixture of gases in Earth's atmosphere. Only nitrogen, oxygen, and argon are considered for atmospheric gases. Other gases are considered negligible in the atmosphere for this analysis.

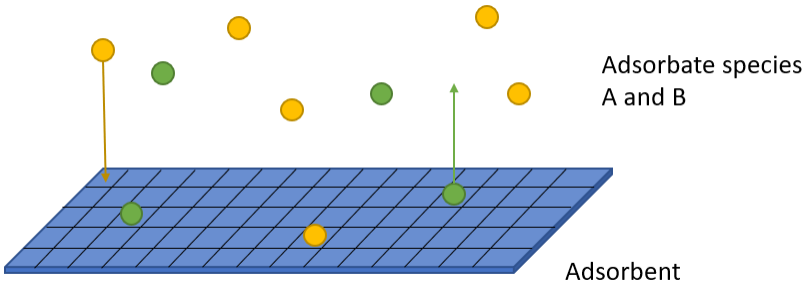

Figure 3.5: ELI Adsorption model of a mixture with 2 adsorbate species.

$$\theta_{N_2} = \frac{K_{N_2}P_{N_2}}{1+K_{N_2}P_{N_2}+K_{O_2}P_{O_2}+K_{Ar}P_{Ar}+K_{CO_2}P_{CO_2}} \tag{III.35}$$

$$\theta_{N_2} = \frac{q_{N_2}}{q_{N_2,max}} \tag{III.36}$$

$$\theta_{O_2} = \frac{K_{O_2}P_{O_2}}{1 + K_{N_2}P_{N_2} + K_{O_2}P_{O_2} + K_{Ar}P_{Ar} + K_{CO_2}P_{CO_2}} \tag{III.37}$$

$$\theta_{O_2} = \frac{q_{O_2}}{q_{O_2,max}} \tag{III.38}$$

$$\theta_{Ar} = \frac{K_{Ar}P_{Ar}}{1 + K_{N_2}P_{N_2} + K_{O_2}P_{O_2} + K_{Ar}P_{Ar} + K_{CO_2}P_{CO_2}} \tag{III.39}$$

$$\theta_{Ar} = \frac{q_{Ar}}{q_{Ar,max}} \tag{III.40}$$

$$\theta_{CO_2} = \frac{K_{CO_2}P_{CO_2}}{1 + K_{N_2}P_{N_2} + K_{O_2}P_{O_2} + K_{Ar}P_{Ar} + K_{CO_2}P_{CO_2}} \tag{III.41}$$

$$\theta_{CO_2} = \frac{q_{CO_2}}{q_{CO_2,max}} \tag{III.42}$$

where θ_i is the fraction of the adsorbent surface covered with component i, K_i is the equilibrium constant for component i, P_i is the pressure of component i, q_i is the amount of component i adsorbed per unit mass of sorbent, and $q_{i,max}$ is the maximum amount of component i that can be adsorbed by the adsorbate.

The PSA unit is used to increase the amount of CO_2 in the airstream going into the deposition chamber. To quantify the amount of component i in the airstream at State 2 in

Figure 3.2, the mole fraction of the component is calculated using Equation III.44

$$y_i = \frac{q_i}{q_{total}} \tag{III.43}$$

PPM, or parts per million, is often used to describe small amounts of a component in a mixture. The PPM of component *i* in the airstream at State 2 is

$$PPM = y_i * 1,000,000 \tag{III.44}$$

Work per CO_2 Captured Basis Conversion.

The work of the compressor calculated in Equation III.21 needs to be converted to a per mass unit of CO_2 adsorbed.

$$\frac{\dot{W}_{PSA}}{\dot{m}_{CO_2,PSA}} = \frac{\dot{W}_{PSA}}{\dot{m}_{air}} \frac{\dot{m}_{air}}{\dot{m}_{sorbent}} \frac{\dot{m}_{sorbent}}{\dot{m}_{CO_2,PSA}} \tag{III.45}$$

The total net work required per unit mass CO_2 to run the DAC system is

$$\frac{\dot{W}_{in}}{\dot{m}_{CO_2,i}} = \frac{\dot{W}_{PSA}}{\dot{m}_{CO_2,PSA}} + \frac{|\dot{W}_c|}{\dot{m}_{CO_2,i}} \tag{III.46}$$

Chapter IIII

Results

Energy Benefit of Precompression for Cryogenic DAC

In this section, results are presented for the NC case, which represents no precompression (n = 1), and cases for three representative compression ratios, n = 400, 800, and 2000, with (TR) and without turbine recovery (PC). The value n = 400 represents a compression ratio that may be obtained with off-the-shelf compressors, such as those used for scuba gear, firefighter breathing equipment, compressed air energy storage, blow molding manufacturing processes, and leak testing of hydraulic and pneumatic systems. A compression ratio of 800 can be obtained with specialized equipment. Finally, a compression ratio of 2000 represents a future-looking aspirational technology target. It is important to note that perfect isothermal compression is assumed, while realistically, one can achieve near-isothermal compression via the addition of intercoolers. There is an added energy cost associated with the addition of the heat exchangers, which is neglected in the present analysis. Therefore, the net work presented here for PC and TR represent best-case scenarios, and the real situation will require a multi-stage compressor with intermediate intercoolers, which is added equipment with an additional energy cost.

As mentioned earlier, pure CO_2 at 1 atm desublimates at -78.5 °C. For partial pressures of CO_2 below 1 atm, however, the lower the concentration of CO_2, the lower the temperature required for desublimation. For the calculations, required target temperatures to desublimate specified mass fractions were needed as input to determine cryogenic cooling loads (Eqs. (III.4) and (III.9)). Figure 4.1 has been prepared to show the temperatures required to desublimate target mass fractions for various compression ratios. As can be seen in the figure, the NC case (n = 1) requires significantly lower temperatures than when the air is compressed to desublimate the same mass fraction of CO_2, hence further illus-

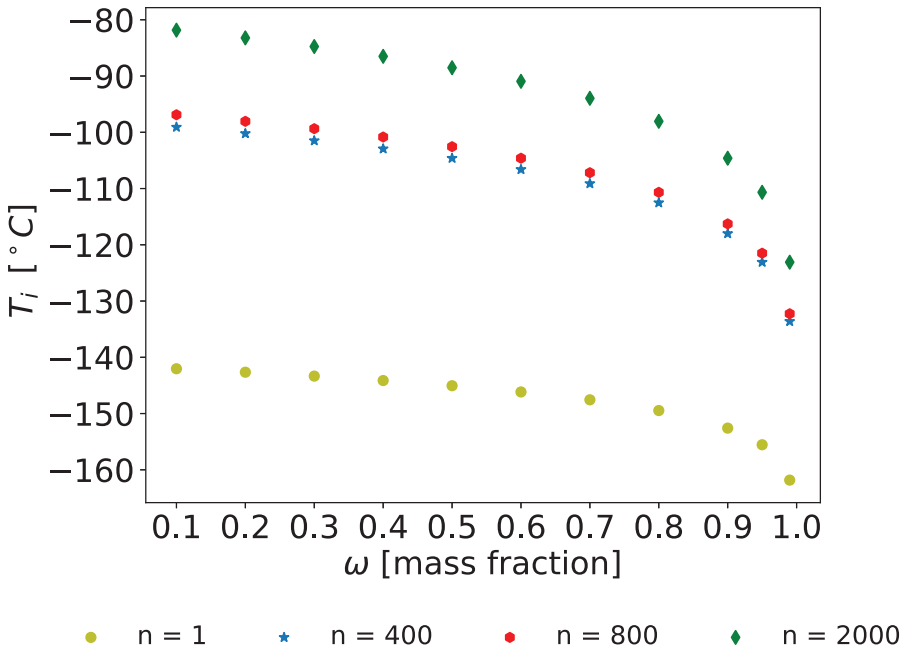

Figure 4.1: Temperature required to desublimate mass fraction ω of CO_2 for various compression ratios

trating the need for the present investigation to determine whether the savings in cooling load outweighs the energy cost of compression. The targeted CO_2 desublimated mass fraction becomes a key variable to optimize because it combines temperature with amount of resultant CO_2 capture.

As a baseline, Figure 4.2 shows the work required for the NC case (Figure 3.1a using a precooler with a heat exchanger effectiveness, ε, equal to 0.7 to desublimate various mass fractions of CO_2. The value 0.7 represents a well-performing heat exchanger. Achieving greater heat exchanger effectiveness often requires costly designs. As seen in Figure 4.2, as the target CO_2 desublimation mass fraction, ω, increases, the work per unit mass of CO_2 decreases, that is, until ω reaches a minimum of 0.9. Attempting to desublimate larger mass fractions results in larger energy penalties due the fact that it takes increasingly lower temperatures to desublimate increasingly smaller amounts of CO_2. In other words,

attempting to remove the last tiny fraction of CO_2 out of the air is not worth the cost of cooling the air further. It is noted here that the figures for all other heat exchanger effectivenesses follow the same trend.

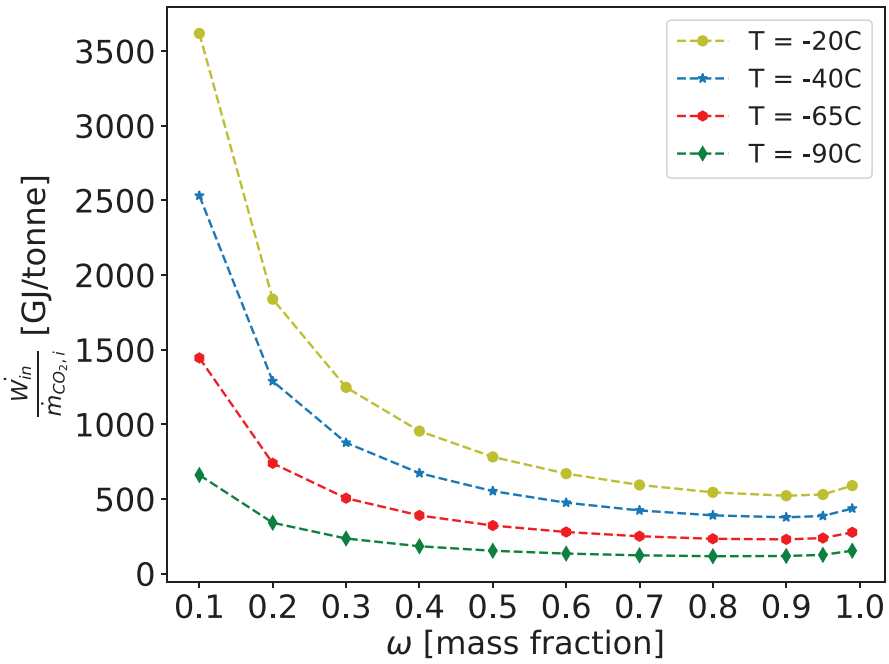

Figure 4.2: Total work required for the no compression case (NC) (Figure 3.1a) to desublimate CO_2 at various inlet temperatures with a precooler effectivess of $\varepsilon = 0.7$

It was found that for all cases of compression ratios and ambient inlet temperatures, precompression acting alone (PC, Figure 3.1b) is never beneficial even for idealized conditions. Therefore, for the real-life case where intercoolers will be needed (adding maintentance costs and energy expenses), precompression acting alone will require even more work than the idealized case. However, there are some cases where there may be a net-energy benefit to employing precompression with turbine recovery (TR, Figure 3.1c). Of the various inlet ambient temperatures, it was found that T_1 = -20 $^\circ$ C had the most scenarios where the possibility of precompression with turbine recovery could potentially be beneficial.

Table 4.1 shows the comparative percentage of work per mass CO_2 required to desublimate a mass fraction ω of CO_2 between TR and NC as a function of heat exchanger effectiveness and compression ratio for an ambient inlet temperature of -20 °C. It is important to note here that when $\varepsilon = 0$ there is no precooler present in the system. The grayed-out space for $\varepsilon \geq 0.6$ represents cases where the precooler gets cold enough to cause the CO_2 to desublimate in the passages of the heat exchangers, thus creating fouling and other complications.

As can be seen in Table 4.1, as the compression ratio increases, there are a larger number of design-space points that could benefit by adding a precompressor with turbine recovery. However, the table only shows the percent differences between two cases for a particular ω and ε and not the overall comparison with regard to what system desublimates the largest mass fraction of CO_2 for the lowest energy cost. It can be seen from the table, that precompression with turbine recovery is most beneficial for systems with no precooler or precoolers with low heat exchanger effectivenesses and low target mass fractions. According to Fig. 4.2, DAC systems should operate in the range of $\omega \sim 0.9$, and it appears that precompression with turbine recovery is only beneficial if no precooler heat exchanger is present. However, as stated previously, intercoolers, which are heat exchangers, are needed for isothermal compression anyway.

Table 4.2 is used to compare the effect of the precooler with a heat exchanger effectiveness of 0.7 (a value that is considered for a well-performing heat exchanger and, for most cases, does not cause fouling—often, increasing the effectiveness of an industrial-size heat exchanger is not worth the added cost) acting alone to compression with turbine recovery if no precooler is present for n = 400, 800, and 2000 at T_1 = -20 °C, -40 °C, -65 °C, and -90 °C. There is no value for n = 2000 at T = -90 °C because this case went beyond the range of NIST REFPROP. As the compression ratio increases, the work input required for TR decreases; however, the cases with no compressor and turbine and only a well-performing

precooler have much less work input. It takes between 175-290% more work to run the system with a precompressor and turbine than it is to run it with the heat exchanger. It is also noted that as T_1 decreases, the percent differences between the cases increases, indicating that the system utilizing TR should be run at higher inlet temperatures. As Table 4.2 shows, if the choice is given between a compression/recovery system and a precooler, it always advantageous to use the precooler alone.

Although it has been determined that, even at the low concentrations of CO_2 found in the atmosphere, implementing precompression and turbine recovery is not feasible, from both a thermodynamics perspective and potentially a cost/maintenance standpoint, it is worthwhile to look at some trends comparing precompression with and without turbine recovery against the system with precooling only. Figure 4.3 has been prepared to show the factor increase of work required for both the PC case and TR case, compared to the baseline NC cases for various compression ratios and target CO_2 desublimation mass fractions for a system with a precooler with $\varepsilon = 0.7$. The factor increase of 1.0 is marked with a black dotted line. This is to note that if any of the bars are below this line, the work to run the system is less than the NC case. It is noted at some values of ω, the data are not included. As previously stated, for those cases, the precooling heat exchanger causes the inlet air temperature, T_2, to fall below the corresponding CO_2 desublimation temperature, causing the CO_2 to prematurely solidify before entering the deposition chamber. As can be seen from the figure, precompression with or without turbine recovery always requires more energy than its corresponding no precompression case. A trend can be noted as the ambient temperature decreases, utilizing precompression and turbine recovery requires more energy to run each system.

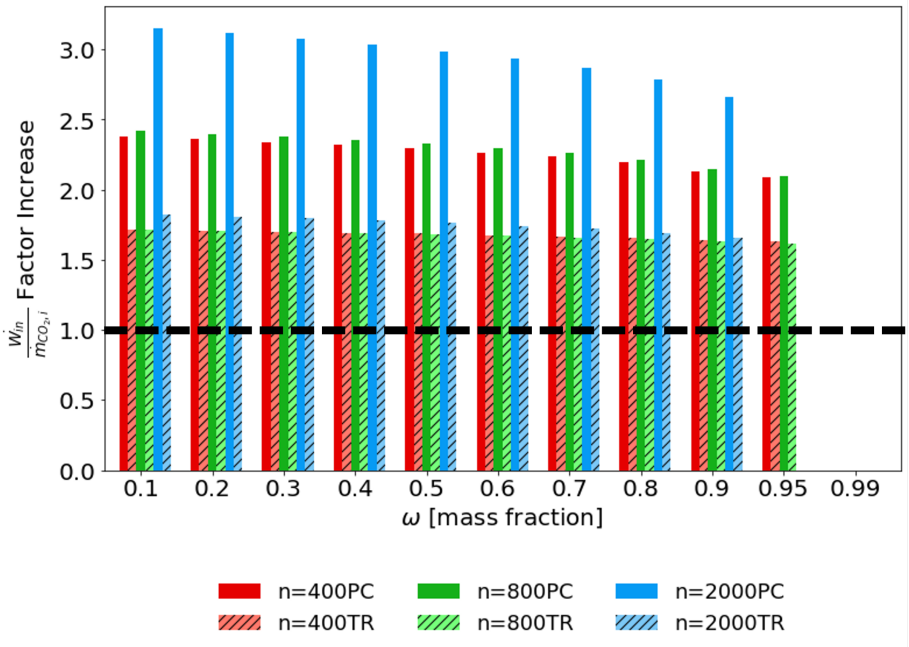

(a) e=0.7 T=-20C TIMESMORE

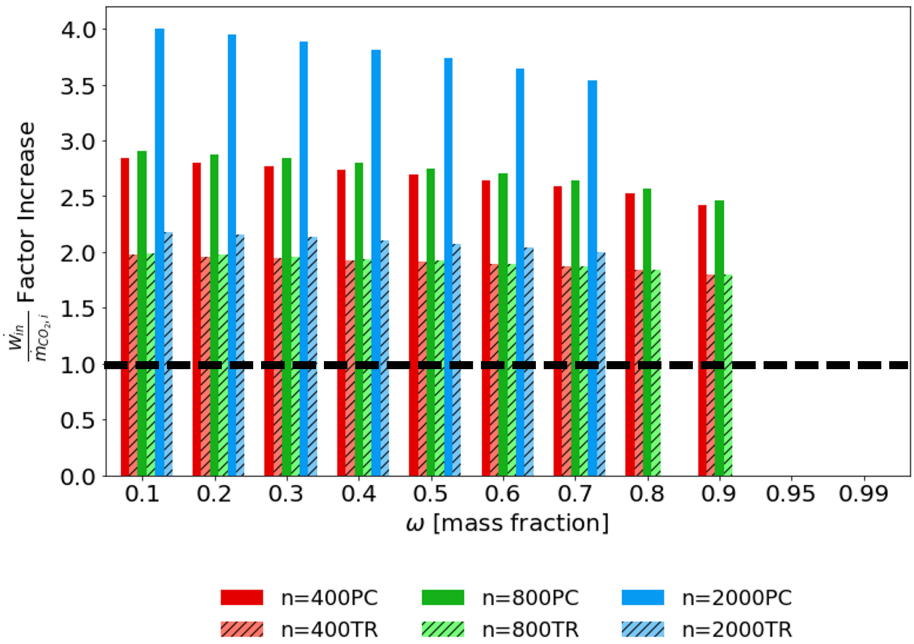

(b) e=0.7 T=-40C TIMESMORE

Figure 4.3: Factor increase of work required for both the PC and TR cases, compared to the baseline NC case, all utilizing a precooler with $\varepsilon = 0.7$ and ambient temperatures of (a) -20 °C, (b) -40 °C, and (c) -65 °C. For each value of ω, from left to right, the first set of bars represents $n = 400$, the second set of bars represents $n = 800$, and the third set of bars represents $n = 2000$.

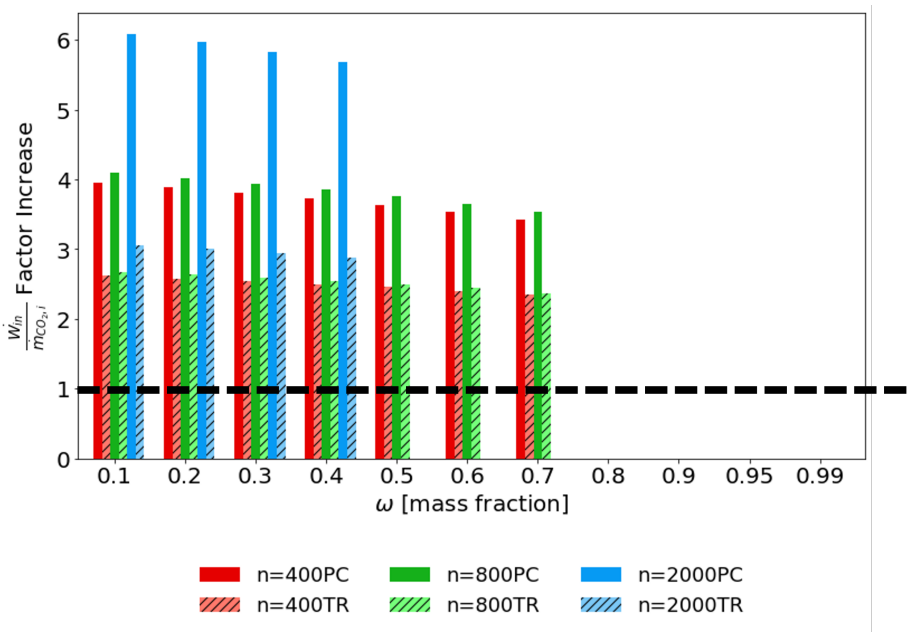

(c) e=0.7 T=-65C TIMESMORE

Figure 4.3: Factor increase of work required for both the PC and TR cases, compared to the baseline NC case, all utilizing a precooler with $\varepsilon = 0.7$ and ambient temperatures of (a) -20 °C, (b) -40 °C, and (c) -65 °C. For each value of ω, from left to right, the first set of bars represents $n = 400$, the second set of bars represents $n = 800$, and the third set of bars represents $n = 2000$.

PSA Combination DAC

In this section, the results are presented for the PSA case. The energy consumption of a PSA unit is conditional to the sorbent material selected. Adsorption constants K and $q_{i,max}$ are found experimentally using adsorption analyzer instrumentation. For this analysis, Zeolite 13X is selected to compare the energy to run a combined PSA-cryogenic distillation carbon capture system (PSA case) versus a cryogenic distillation system alone (NC case). Adsorption isotherms for Zeolite 13X at T_{amb} = -50°C used in this analysis are found in Table 4.3. The PSA unit simulated a CO_2 increase from ambient concentrations to 7,000 ppm. An ideal case represented in this analysis uses a simple dual-column configuration to produce a continuous flow between the adsorption and desorption steps. In the real case, a multi dual-column setup may be utilized to meet operating conditions and flow rates, adding to the equipment and overall energy cost.

Figure 4.4 shows the required energy input per mass of CO_2 captured to run the NC case (black) and the PSA case (purple), evaluated at ε_{HX} = 0.7. The heat exchanger effectiveness was selected to maximize efficiency without suffering fouling in the heat exchanger channels. As seen in the graph, it is approximately half the energy intensity to the run the PSA system compared to the NC system across all mass fractions. Increasing the inlet CO_2 concentration to the deposition chamber significantly reduces the energy to run the system. A thermodynamic minimum was found at ω = 0.9 of 143 GJ/tonne CO_2 captured. This energy consumption is considerably higher than reported energy consumption of other DAC systems [Boetcher et al., 2019]. However, improvements to cryogenic distillation component efficiency and overall system optimizations may drive the energy cost down to a competitive value.

The effect of inlet CO_2 concentration on cryocooler work was evaluated at 400, 1,000, and 7,000 ppm. A value of 400 ppm constitutes ambient atmospheric concentrations of CO_2. A value of 1,000 ppm represents experimental CO_2 concentration increases using

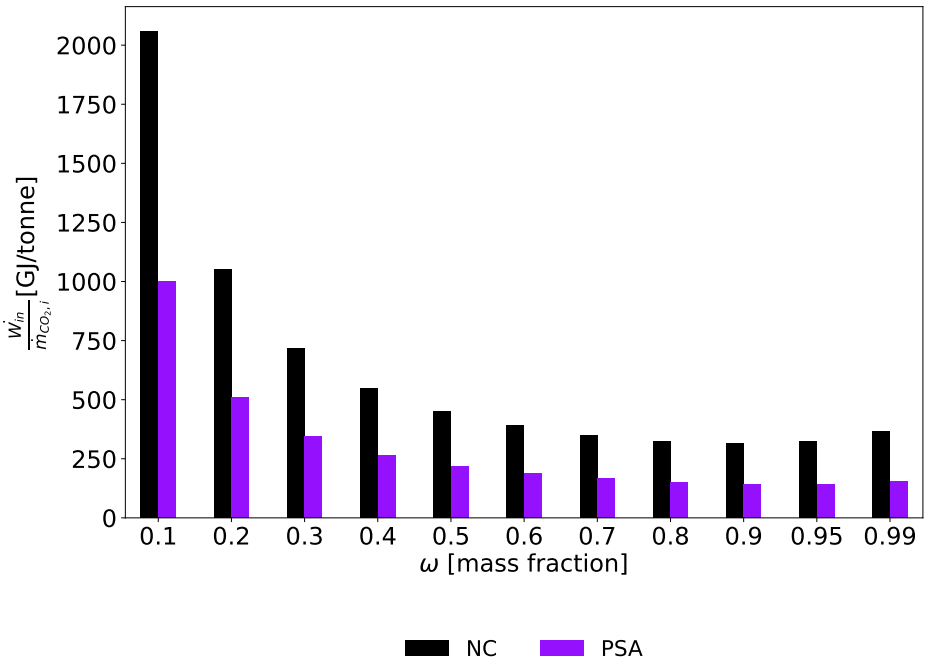

Figure 4.4: Total work required to run PSA versus NC at various mass fractions at a heat exchanger effectiveness $\varepsilon = 0.7$.

Zeolite 13X. A value of 7,000 ppm reflects a theoretical concentration increase using Langmuir adsorption isotherms from the modeled PSA unit. Figure 4.5 is prepared to show the result of increasing the inlet CO_2 concentration on the work input to the cryocooler, W_r. As the inlet concentration rises, W_r significantly decreases. Almost doubling the inlet concentration (from 400 ppm to 1,000 ppm) lowers the energy consumption by approximately 60%. This concludes that varying the inlet CO_2 concentration greatly influences the overall energy cost of the system and future endeavours should prioritize this phenomena when designing DAC systems.

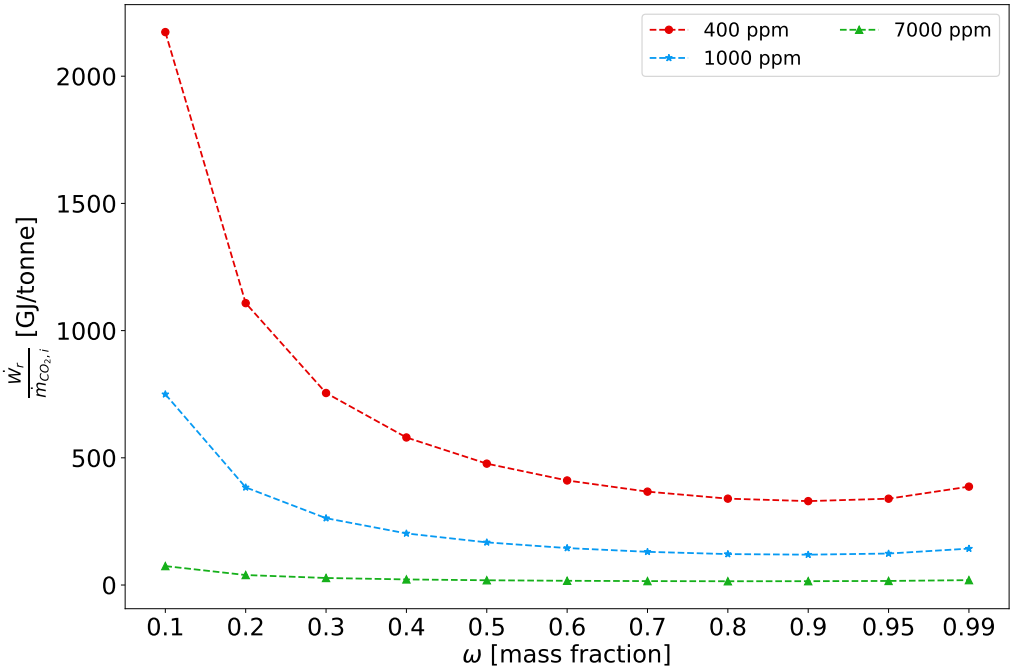

Figure 4.5: Work input to the cryocooler as the inlet CO_2 concentration is varied.

To get a better understanding of the breakdown of energy consumption in the PSA case (Figure 3.2b), the work input to the PSA unit, W_{PSA} (blue), and the work input to the cryocooler, W_r (red), are compared in Figure 4.6. It is noted that W_r is a function of ω, whereas W_{PSA} does not change with ω. As seen in the graph, W_r contributes to the overwhelming majority of the energy cost for the combined system. The bulk of the energy demand originates from maintaining an ultra-low temperature environment where desublimation of dilute concentrations of CO_2 occurs.

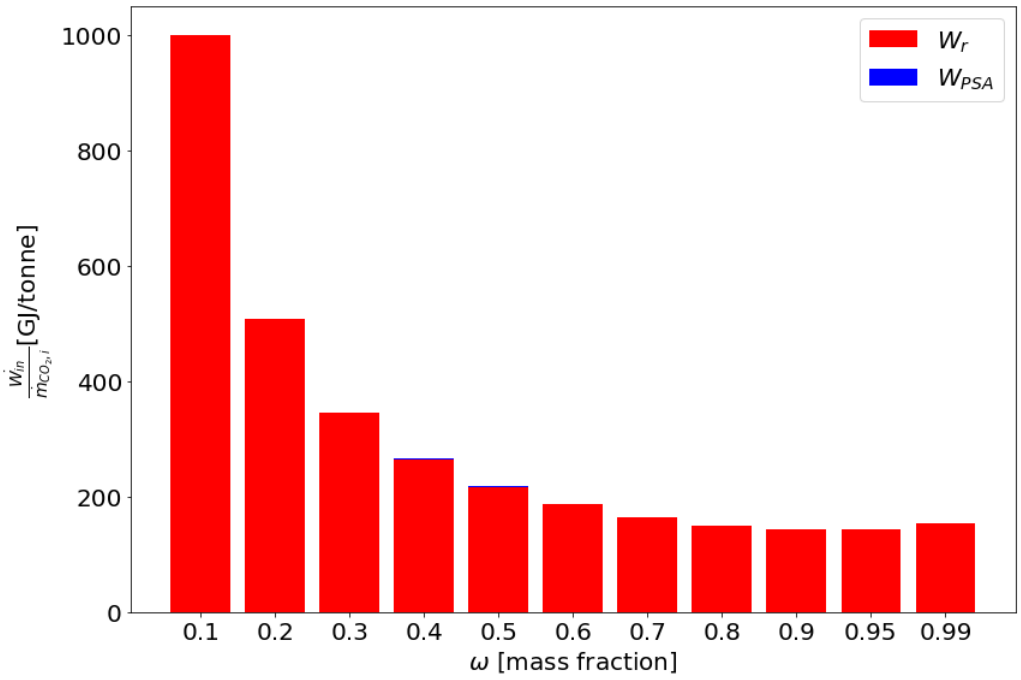

Figure 4.6: Work of the cryocooler (red) and work of the PSA unit (blue) at $\varepsilon = 0.7$.

Table 4.1: Comparison of total work, by percentage, required to run the system with pre-compression and turbine recovery (TR, Figure 3.1c) compared to the no compression system (NC, Figure 3.1a) at T_1 = -20 °C for n = 400, 800, and 2000. A positive percentage means that TR takes more work than the corresponding NC case, and a negative percentage means TR takes less work than the corresponding NC case

n = 400

$\omega\varepsilon$	**0**	**0.1**	**0.2**	**0.3**	**0.4**	**0.5**	**0.6**	**0.7**	**0.8**	**0.9**	**0.95**
0.99	10.1	13.2	16.8	21.1	26.5	33.8	44.4				
0.95	4.4	7.7	11.6	16.4	22.6	30.9	43.1	62.9			
0.9	1.7	5.1	9.2	14.3	20.8	29.7	42.7	64.0			
0.8	*-1.2*	2.4	6.7	12.1	19.0	28.6	42.5	65.5	110.8		
0.7	*-2.9*	0.8	5.2	10.8	18.0	28.0	42.6	66.7	114.2		
0.6	*-4.2*	*-0.4*	4.2	9.9	17.4	27.6	42.8	67.7	117.0	262.5	
0.5	*-5.2*	*-1.3*	3.4	9.2	16.9	27.4	42.9	68.6	119.3	269.5	
0.4	*-6.0*	*-2.1*	2.7	8.7	16.5	27.2	43.1	69.4	121.4	275.7	
0.3	*-6.6*	*-2.7*	2.1	8.2	16.2	27.1	43.4	70.2	123.3	281.3	592.7
0.2	*-7.2*	*-3.2*	1.7	7.8	15.9	27.1	43.6	70.9	125.1	286.6	606.1
0.1	*-7.8*	*-3.7*	1.3	7.5	15.7	27.0	43.8	71.6	126.7	291.4	619.0

n = 800

$\omega\varepsilon$	**0**	**0.1**	**0.2**	**0.3**	**0.4**	**0.5**	**0.6**	**0.7**	**0.8**	**0.9**	**0.95**
0.99	6.0	9.0	12.6	17.1	22.7	30.3	41.4				
0.95	0.4	3.7	7.7	12.6	19.0	27.7	40.5	61.4			
0.9	*-2.2*	1.3	5.4	10.7	17.4	26.7	40.4	62.8			
0.8	*-4.9*	*-1.3*	3.1	8.7	15.9	25.8	40.5	64.7	112.3		
0.7	*-6.6*	*-2.8*	1.8	7.5	15.0	25.4	40.8	66.1	116.1		
0.6	*-7.8*	*-3.9*	0.8	6.7	14.5	25.2	41.1	67.3	119.1		
0.5	*-8.7*	*-4.7*	0.1	6.1	14.1	25.1	41.4	68.3	121.7	279.8	
0.4	*-9.4*	*-5.4*	*-0.5*	5.7	13.8	25.0	41.7	69.3	124.0	286.4	
0.3	*-10.0*	*-6.0*	*-1.0*	5.3	13.6	25.0	42.0	70.2	126.1	292.4	620.0
0.2	*-10.6*	*-6.5*	*-1.4*	5.0	13.4	25.0	42.4	71.0	128.1	297.9	634.2
0.1	*-11.1*	*-6.9*	*-1.8*	4.7	13.2	25.1	42.7	71.8	129.9	303.1	647.8

n = 2000

$\omega\varepsilon$	**0**	**0.1**	**0.2**	**0.3**	**0.4**	**0.5**	**0.6**	**0.7**	**0.8**	**0.9**	**0.95**
0.99	*-8.9*	*-5.4*	*-1.2*	4.1	11.1	20.7					
0.95	*-14.1*	*-10.3*	*-5.5*	0.5	8.4	19.4	35.7				
0.9	*-16.4*	*-12.4*	*-7.3*	*-0.9*	7.5	19.2	36.6	65.4			
0.8	*-18.7*	*-14.4*	*-9.0*	*-2.2*	6.9	19.5	38.2	69.2			
0.7	*-20.0*	*-15.5*	*-9.9*	*-2.8*	6.7	19.8	39.4	71.9	136.3		
0.6	*-20.9*	*-16.2*	*-10.5*	*-3.1*	6.7	20.3	40.5	74.1	140.9		
0.5	*-21.5*	*-16.8*	*-10.9*	*-3.3*	6.7	20.7	41.5	76.1	144.8		
0.4	*-22.1*	*-17.2*	*-11.1*	*-3.4*	6.8	21.1	42.4	77.8	148.2	357.4	
0.3	*-22.5*	*-17.5*	*-11.4*	*-3.5*	7.0	21.5	43.3	79.4	151.4	365.6	
0.2	*-22.8*	*-17.8*	*-11.5*	*-3.5*	7.1	21.9	44.1	80.9	154.2	373.1	806.5
0.1	-23.1	*-18.0*	*-11.6*	*-3.5*	7.3	22.3	44.8	82.3	156.9	380.1	824.2

Table 4.2: Percent differences in work required to run the system between TR (Figure 3.1c) and no precooler ($\varepsilon = 0$) and NC (Figure 3.1a) with a precooler ($\varepsilon = 0.7$) for various compression ratios and inlet temperatures.

	TR ε **= 0**	**NC** ε **= 0.7**	**Percent difference**
	$\frac{\dot{W}_{in}}{\dot{m}_{CO_2,i}}$ [GJ/tonne]	$\frac{\dot{W}_{in}}{\dot{m}_{CO_2,i}}$ [GJ/tonne]	[%]
n		**T_1 = -20 °C**	
400	1746	521	235
800	1680	521	222
2000	1435	521	175
		T_1 = -40 °C	
400	1271	377	237
800	1224	377	225
2000	1059	377	181
		T_1 = -65 °C	
400	794	229	247
800	768	229	235
2000	693	229	203
		T_1 = -90 °C	
400	455	117	289
800	448	117	283
2000	-	117	-

Table 4.3: Adsorption isotherm constants for Zeolite 13X at -50°C

Component		**K (Pa)**	**$q_{i,max}$ (mol/g)**
Nitrogen	N_2	2.301	2.209 x 10^{-3}
Oxygen	O_2	1.121	2.67 x 10^{-5}
Argon	Ar	1.434	3.33 x 10^{-3}
Carbon Dioxide	CO_2	15.92	4.37 x 10^{-3}

Chapter V

Conclusions

Global anthropogenic GHG emissions are at an all time high and are directly causing climate change. The concentration of CO_2 in the atmosphere has increased almost 40% over the past two centuries, leading to unimaginable negative effects on the planet. Earth's average temperature is increasing every year and scientists have warned of catastrophic disaster if the temperature increases 2°C above pre-industrial levels. The scientific community agrees that through the reduction of GHG emissions, electrification and decarbonization of various sectors, and CO_2 removal activities, climate change can be alleviated.

Direct air capture of CO_2 is one of the many climate change mitigation strategies needed to reverse global warming. Direct air capture requires specialized systems to capture dilute CO_2 concentrations from atmospheric air conditions. DAC can be accomplished through different mechanisms such as cryogenic distillation, adsorption, absorption, and membrane separation. DAC has potential for large scale operation however requires more analysis to increase development rates.

The results of this study extend the analysis of Boetcher et al. [Boetcher et al., 2019] and [Perskin et al., 2022] in thermodynamically modeling a DAC system under different parameters and preconditions. A thermodynamic model was constructed using psychometric theories to model the desublimation of CO_2 in a DAC system. The system was modeled to include a precooling heat exchanger and a deposition chamber where the desublimation of CO_2 occurs. Three base systems were studied, NC (no precompression or turbine recovery), PC (precompression only), and TR (precompression and turbine recovery) at three different compression ratios, n = 400, 800, and 2000. Then, a combination DAC system, PSA (pressure swing adsorption and cryogenic distillation), was modeled. A dual-column, 4-step Skarstrom Cycle PSA unit was analyzed using Extended Langmuir Models and the

ideal gas law to simulate a CO_2 concentration prior to the deposition chamber. The NC and PSA systems were evaluated at T_{amb} = -50°C.

This study finds that while increasing the compression ratio of the system, there is no net energy benefit when capturing CO_2 given the current state-of-the-art in commercial compressor and cryocooler capabilities. The assessment of the efficiency of a precooler versus TR finds that it is more advantageous to utilize a heat exchanger precooler than pre-compression with turbine recovery in a DAC system. Combining DAC systems may yield a more efficient system. PSA combined with cryogenic capture is less energy intensive than cryogenic capture alone. In a combined DAC system with PSA and cryogenic distillation, the PSA unit has a significantly lower energy consumption than the cryocooler. Increasing the concentration of CO_2 entering the deposition chamber significantly decreases the required energy consumption of the cryocooler.

Future Recommendations

The novelty in this research lies in the preliminary modeling of a cryogenic DAC system and the combination DAC system. It is important to note that the work here represents an ongoing proof-of-concept theoretical analysis to determine energy requirements for DAC in arctic/Antarctic climates. Many assumptions are made in the present study that should be investigated further to provide a more robust energy analysis of direct air capture systems.

Exploration and development of the components in the system are crucial to performance. The dimensions of the PSA unit chamber are not taken into consideration in this study. The effect of height, depth, and length of the adsorption chamber should be modeled to optimize adsorption performance. The effectiveness of the heat exchanger is a significant component to reduce the energy consumption of the total system. Priority should be taken to design the configuration of an efficient heat exchanger that maximizes heat transfer without incurring ice accumulation (fouling) for cryogenic flow. Additionally, research

and development into the deposition chamber must occur to capture the CO_2. The process of transporting the solid CO_2 from the deposition chamber to a storage unit to allow continuous air flow throughout the system should also be considered.

The results of the case study conclude that the combination DAC system is less energy intensive than a single DAC system. One can conclude that combining other DAC mechanisms such as temperature swing adsorption, membrane separation, or chemical absorption with the established cryongenic distillation and/or pressure swing adsorption can reduce the energy consumption even further.

References

[Aaron and Tsouris, 2005] Aaron, D. and Tsouris, C. (2005). Separation of CO_2 from flue gas: A review. *Separation Science and Technology*, 40(1-3):321–348.

[Abd et al., 2020] Abd, A. A., Naji, S. Z., Hashim, A. S., and Othman, M. R. (2020). Carbon dioxide removal through physical adsorption using carbonaceous and non-carbonaceous adsorbents: A review. *Journal of Environmental Chemical Engineering*, 8(5):104142.

[Agarwal, 2010] Agarwal, A. (2010). *Advanced strategies for optimal design and operation of pressure swing adsorption processes*. PhD thesis. Copyright - Database copyright ProQuest LLC; ProQuest does not claim copyright in the individual underlying works; Last updated - 2023-03-03.

[Agee et al., 2013] Agee, E., Orton, A., and Rogers, J. (2013). CO_2 snow deposition in Antarctica to curtail anthropogenic global warming. *J. App. Meteor. & Climat.*, 52:281–288.

[Agee and Orton, 2016] Agee, E. M. and Orton, A. (2016). An initial laboratory prototype experiment for sequestration of atmospheric CO_2. *Journal of Applied Meteorology and Climatology*, 55(8):1763–1770.

[Bao et al., 2022] Bao, J., Zhao, J., and Bi, X. T. (2022). CO_2 adsorption and desorption for CO_2 enrichment at low-concentrations using zeolite 13x. *Chemie Ingenieur Technik*, 95(1-2):143–150.

[Baxter et al., 2009] Baxter, L., Baster, A., and Burt, S. (2009). Cryogenic CO_2 capture as a cost effective CO_2 process. In *International Pittsburgh Coal Conference*.

[Boetcher et al., 2019] Boetcher, S. K. S., Traum, M. J., and von Hippel, T. (2019). Thermodynamic model of CO_2 deposition in cold climates. *Climatic Change*, 158(3-4):517–530.

[Burt et al., 2009] Burt, S., Baxter, A., and Baxter, L. (2009). Cryogenic CO_2 capture to control climate change emissions. In *Proceedings of the 34th International Technical Conference on Clean Coal & Fuel Systems*.

[Chan et al., 1981] Chan, Y. N. I., Hill, F. B., and Wong, Y. W. (1981). Equilibrium theory of a pressure swing adsorption process. *Chemical Engineering Science*, 36(2):243–251.

[Choi et al., 2011] Choi, S., Gray, M. L., and Jones, C. W. (2011). Amine-tethered solid adsorbents coupling high adsorption capacity and regenerability for CO_2 capture from ambient air. *ChemSusChem*, 4(5):628–635.

[Chue et al., 1995] Chue, K. T., Kim, J. N., Yoo, Y. J., Cho, S. H., and Yang, R. T. (1995). Comparison of activated carbon and zeolite 13x for CO_2 recovery from flue gas by pressure swing adsorption. *Industrial &amp Engineering Chemistry Research*, 34(2):591–598.

[Commission, 2022] Commission, C. E. (2022). 2022 building energy efficiency standards.

[Davis et al., 2018] Davis, S. J., Lewis, N. S., Shaner, M., Aggarwal, S., Arent, D., Azevedo, I. L., Benson, S. M., Bradley, T., Brouwer, J., Chiang, Y.-M., Clack, C. T. M., Cohen, A., Doig, S., Edmonds, J., Fennell, P., Field, C. B., Hannegan, B., Hodge, B.-M., Hoffert, M. I., Ingersoll, E., Jaramillo, P., Lackner, K. S., Mach, K. J., Mastrandrea, M., Ogden, J., Peterson, P. F., Sanchez, D. L., Sperling, D., Stagner, J., Trancik, J. E., Yang, C.-J., and Caldeira, K. (2018). Net-zero emissions energy systems. *Science*, 360(6396).

[Dey et al., 2022] Dey, A., Dash, S. K., and Mandal, B. (2022). Introduction to carbon capture. In *Emerging Carbon Capture Technologies*, pages 1–31. Elsevier.

[DoE, 2022] DoE (2022). Pre-combustion carbon capture research.

[EPA, 2022] EPA (2022). Overview of greenhouse gases.

[EPA, 2023] EPA (2023). Electric vehicle myths.

[Font-Palma et al., 2021] Font-Palma, C., Cann, D., and Udemu, C. (2021). Review of cryogenic carbon capture innovations and their potential applications. *C*, 7(3):58.

[Forster et al., 2007] Forster, P., Ramaswamy, V., Artaxo, P., Berntsen, T., Betts, R., Fahey, D. W., Haywood, J., Lean, J., Lowe, D. C., Myhre, G., Nganga, J., Prinn, R., Raga, G., Schulz, M., and Van Dorland, R. (2007). Changes in atmospheric constituents and in radiative forcing. In Solomon, S., Qin, D., Manning, M., Chen, Z., Marquis, M., Averyt, K. B., Tignor, M., and Miller, H. L., editors, *Climate Change 2007: The Physical Science Basis. Contribution of Working Group I to the Fourth Assessment Report of the Intergovernmental Panel on Climate Change*, book section 2. Cambridge University Press, Cambridge, United Kingdom and New York, NY, USA.

[Gargiulo et al., 2020] Gargiulo, N., Peluso, A., and Caputo, D. (2020). MOF-based adsorbents for atmospheric emission control: A review. *Processes*, 8(5):613.

[Grande, 2012] Grande, C. A. (2012). Advances in pressure swing adsorption for gas separation. *ISRN Chemical Engineering*, 2012:1–13.

[Gür, 2022] Gür, T. M. (2022). Carbon dioxide emissions, capture, storage and utilization: Review of materials, processes and technologies. *Progress in Energy and Combustion Science*, 89:100965.

[Hao et al., 2011] Hao, G.-P., Li, W.-C., Qian, D., Wang, G.-H., Zhang, W.-P., Zhang, T., Wang, A.-Q., Schüth, F., Bongard, H.-J., and Lu, A.-H. (2011). Structurally designed synthesis of mechanically stable poly(benzoxazine-co-resol)-based porous car-

bon monoliths and their application as high-performance CO_2 capture sorbents. *Journal of the American Chemical Society*, 133(29):11378–11388.

[House et al., 2009] House, K. Z., Harvey, C. F., Aziz, M. J., and Schrag, D. P. (2009). The energy penalty of post-combustion CO_2 capture & storage and its implications for retrofitting the u.s. installed base. *Energy &amp Environmental Science*, 2(2):193.

[Hu et al., 2018] Hu, Z., Wang, Y., Shah, B. B., and Zhao, D. (2018). COsub2/sub capture in metal-organic framework adsorbents: An engineering perspective. *Advanced Sustainable Systems*, 3(1):1800080.

[Humpenöder et al., 2014] Humpenöder, F., Popp, A., Dietrich, J. P., Klein, D., Lotze-Campen, H., Bonsch, M., Bodirsky, B. L., Weindl, I., Stevanovic, M., and Müller, C. (2014). Investigating afforestation and bioenergy CCS as climate change mitigation strategies. *Environmental Research Letters*, 9(6):064029.

[IEA, 2022a] IEA (2022a). Direct air capture.

[IEA, 2022b] IEA (2022b). Renewable power generation by technology in the net zero scenario, 2010-2030 charts – data and statistics.

[IEA, 2022c] IEA (2022c). Solar pv – analysis.

[IEA, 2023] IEA (2023). Renewables - fuels and technologies.

[IPCC, 2014a] IPCC (2014a). Anthropogenic and natural radiative forcing. In *Climate Change 2013 – The Physical Science Basis*, pages 659–740. Cambridge University Press.

[IPCC, 2014b] IPCC (2014b). Carbon and other biogeochemical cycles. In *Climate Change 2013 – The Physical Science Basis*, pages 465–570. Cambridge University Press.

[IPCC, 2018] IPCC (2018). Summary for policymakers in global warming of 1.5°c. an ipcc special report on the impacts of global warming of 1.5°c above pre-industrial levels and related global greenhouse gas emission pathways, in the context of strengthening the global response to the threat of climate change, sustainable development, and efforts to eradicate poverty. Cambridge University Press.

[IPCC, 2022] IPCC (2022). Climate change 2022: Mitigation of climate change contribution of working group iii to the sixth assessment report of the intergovernmental panel on climate change. *Climate Change 2022*.

[Kroposki et al., 2017] Kroposki, B., Johnson, B., Zhang, Y., Gevorgian, V., Denholm, P., Hodge, B.-M., and Hannegan, B. (2017). Achieving a 100% renewable grid: Operating electric power systems with extremely high levels of variable renewable energy. *IEEE Power and Energy Magazine*, 15(2):61–73.

[Kumar et al., 2015] Kumar, A., Madden, D. G., Lusi, M., Chen, K.-J., Daniels, E. A., Curtin, T., Perry, J. J., and Zaworotko, M. J. (2015). Direct air capture of CO_2 by physisorbent materials. *Angewandte Chemie International Edition*, 54(48):14372–14377.

[Lackner et al., 1999] Lackner, K., Ziock, H.-J., and Grimes, P. (1999). Carbon dioxide extraction from air: Is it an option?

[Lackner, 2013] Lackner, K. S. (2013). The thermodynamics of direct air capture of carbon dioxide. *Energy*, 50:38–46.

[Lai et al., 2021] Lai, J. Y., Ngu, L. H., and Hashim, S. S. (2021). A review of CO_2 adsorbents performance for different carbon capture technology processes conditions. *Greenhouse Gases: Science and Technology*, 11(5):1076–1117.

[Lemmon et al., 2000] Lemmon, E., Jacobsen, R., Penoncello, S., and Friend, D. (2000). Thermodynamic properties of air and mixtures of nitrogen, argon, and oxygen from 60

to 2000 K at pressures to 2000 MPa. *Journal of Physical and Chemical Reference Data*, 29.

[Lemmon et al., 2018] Lemmon, E. W., Bell, I., Huber, M. L., and McLinden, M. O. (2018). NIST Standard Reference Database 23: Reference Fluid Thermodynamic and Transport Properties-REFPROP, Version 10.0, National Institute of Standards and Technology.

[Leonzio et al., 2022] Leonzio, G., Mwabonje, O., Fennell, P. S., and Shah, N. (2022). Environmental performance of different sorbents used for direct air capture. *Sustainable Production and Consumption*, 32:101–111.

[Li et al., 2016] Li, S., Ding, J., Zhang, Z., Cheng, D., Hu, X., and Li, X. (2016). A feasible energy-saving analysis of a new system for CO_2 cryogenic capture. *International Journal of Low-Carbon Technologies*, 11(2):235–239.

[Liu et al., 2021] Liu, R.-S., Xu, S., Hao, G.-P., and Lu, A.-H. (2021). Recent advances of porous solids for ultradilute CO_2 capture. *Chemical Research in Chinese Universities*, 38(1):18–30.

[Liu et al., 2022] Liu, W., Lin, Y., Ji, Y., Yong, J., Zhang, X., and Jiang, L. (2022). Thermodynamic study on two adsorption working cycles for direct air capture. *Applied Thermal Engineering*, 214:118920.

[Lively and Realff, 2016] Lively, R. P. and Realff, M. J. (2016). On thermodynamic separation efficiency: Adsorption processes. *AIChE Journal*, 62(10):3699–3705.

[Madden et al., 2017] Madden, D. G., Scott, H. S., Kumar, A., Chen, K.-J., Sanii, R., Bajpai, A., Lusi, M., Curtin, T., Perry, J. J., and Zaworotko, M. J. (2017). Flue-gas and direct-air capture of CO_2 by porous metal–organic materials. *Philosophical Transactions of the Royal Society A: Mathematical, Physical and Engineering Sciences*, 375(2084):20160025.

[McQueen et al., 2021] McQueen, N., Gomes, K. V., McCormick, C., Blumanthal, K., Pisciotta, M., and Wilcox, J. (2021). A review of direct air capture (DAC): scaling up commercial technologies and innovating for the future. *Progress in Energy*, 3(3):032001.

[Metz et al., 2005] Metz, B., Davidson, O., Coninck, H. d., Loos, M., and Meyer, L. (2005). Special report on carbon dioxide capture and storage.

[Muana, 2021] Muana (2021). Carbon dioxide peaks near 420 parts per million at Muana Loa observatory, https://research.noaa.gov/article/artmid/587/articleid/2764/coronavirus-response-barely-slows-rising-carbon-dioxide, last accessed august 5, 2022.

[NAP, 1992] NAP (1992). *Policy Implications of Greenhouse Warming: Mitigation, Adaptation, and the Science Base*. The National Academies Press, Washington, DC.

[Nassar et al., 2017] Nassar, R., Hill, T. G., McLinden, C. A., Wunch, D., Jones, D. B. A., and Crisp, D. (2017). Quantifying CO_2 emissions from individual power plants from space. *Geophysical Research Letters*, 44(19).

[NOAA, 2019] NOAA (2019). Carbon cycle.

[Oschatz and Antonietti, 2018] Oschatz, M. and Antonietti, M. (2018). A search for selectivity to enable CO_2 capture with porous adsorbents. *Energy &amp Environmental Science*, 11(1):57–70.

[Ozkan and and, 2022] Ozkan, M. and and, R. C. (2022). The status and prospects of materials for carbon capture technologies. *MRS Bulletin*, 47(4):390–394.

[Perskin et al., 2022] Perskin, J. B., Traum, M. J., von Hippel, T., and Boetcher, S. K. (2022). On the feasibility of precompression for direct atmospheric cryogenic carbon capture. *Carbon Capture Science &amp Technology*, 4:100063.

[Plank and Manning, 2019] Plank, T. and Manning, C. E. (2019). Subducting carbon. *Nature*, 574(7778):343–352.

[Press, 2019] Press, N. A. (2019). *Negative Emissions Technologies and Reliable Sequestration*. National Academies Press.

[Quéré et al., 2016] Quéré, C. L., Andrew, R. M., Canadell, J. G., Sitch, S., Korsbakken, J. I., Peters, G. P., Manning, A. C., Boden, T. A., Tans, P. P., Houghton, R. A., Keeling, R. F., Alin, S., Andrews, O. D., Anthoni, P., Barbero, L., Bopp, L., Chevallier, F., Chini, L. P., Ciais, P., Currie, K., Delire, C., Doney, S. C., Friedlingstein, P., Gkritzalis, T., Harris, I., Hauck, J., Haverd, V., Hoppema, M., Goldewijk, K. K., Jain, A. K., Kato, E., Körtzinger, A., Landschützer, P., Lefèvre, N., Lenton, A., Lienert, S., Lombardozzi, D., Melton, J. R., Metzl, N., Millero, F., Monteiro, P. M. S., Munro, D. R., Nabel, J. E. M. S., ichiro Nakaoka, S., O'Brien, K., Olsen, A., Omar, A. M., Ono, T., Pierrot, D., Poulter, B., Rödenbeck, C., Salisbury, J., Schuster, U., Schwinger, J., Séférian, R., Skjelvan, I., Stocker, B. D., Sutton, A. J., Takahashi, T., Tian, H., Tilbrook, B., van der Laan-Luijkx, I. T., van der Werf, G. R., Viovy, N., Walker, A. P., Wiltshire, A. J., and Zaehle, S. (2016). Global carbon budget 2016. *Earth System Science Data*, 8(2):605–649.

[Radebaugh, 2004] Radebaugh, R. (2004). Refrigeration for superconductors. *Proceedings of the IEEE*, pages 1719–1734.

[Rhodes, 2017] Rhodes, C. J. (2017). The imperative for regenerative agriculture. *Science Progress*, 100(1):80–129.

[Ribeiro et al., 2014] Ribeiro, R. P. P. L., Grande, C. A., and Rodrigues, A. E. (2014). Electric swing adsorption for gas separation and purification: A review. *Separation Science and Technology*, 49(13):1985–2002.

[Ritchie et al., 2020] Ritchie, H., Roser, M., and Rosado, P. (2020). Co and greenhouse gas emissions. *Our World in Data*. https://ourworldindata.org/co2-and-greenhouse-gas-emissions.

[Rochelle, 2009] Rochelle, G. T. (2009). Amine scrubbing for CO_2 capture. *Science*, 325(5948):1652–1654.

[Ruthven, 2014] Ruthven, D. M. (2014). CO_2 capture: Value functions, separative work and process economics. *Chemical Engineering Science*, 114:128–133.

[Sabatino et al., 2021] Sabatino, F., Grimm, A., Gallucci, F., van Sint Annaland, M., Kramer, G. J., and Gazzani, M. (2021). A comparative energy and costs assessment and optimization for direct air capture technologies. *Joule*, 5(8):2047–2076.

[Sanguesa et al., 2021] Sanguesa, J. A., Torres-Sanz, V., Garrido, P., Martinez, F. J., and Marquez-Barja, J. M. (2021). A review on electric vehicles: Technologies and challenges. *Smart Cities*, 4(1):372–404.

[Sanz-Perez et al., 2016] Sanz-Perez, E. S., Murdock, C. R., Didas, S. A., and Jones, C. W. (2016). Direct capture of CO_2 from ambient air. *Chemical Reviews*, 116(19):11840–11876.

[Schach et al., 2011] Schach, M.-O., Oyarzún, B., Schramm, H., Schneider, R., and Repke, J.-U. (2011). Feasibility study of CO_2 capture by anti-sublimation. *Energy Procedia*, 4:1403–1410.

[Shendalman and Mitchell, 1972] Shendalman, L. and Mitchell, J. (1972). A study of heatless adsorption in the model system CO_2 in he, i. *Chemical Engineering Science*, 27(7):1449–1458.

[Sherif and Knox, 2005] Sherif, D. E. and Knox, J. C. (2005). International space station carbon dioxide removal assembly (ISS CDRA) concepts and advancements. In *SAE Technical Paper Series*. SAE International.

[Shi et al., 2022] Shi, X., Lin, Y., and Chen, X. (2022). Development of sorbent materials for direct air capture of CO_2. *MRS Bulletin*, 47(4):405–415.

[Skarstrom, 1958] Skarstrom, C. (1958). Method and apparatus for fractionating gaseous mixtures by adsorption.

[Song et al., 2012] Song, C.-F., Kitamura, Y., Li, S.-H., and Ogasawara, K. (2012). Design of a cryogenic CO_2 capture system based on Stirling coolers. *International Journal of Greenhouse Gas Control*, 7:107–114.

[Sovacool et al., 2022] Sovacool, B. K., Baum, C. M., Low, S., Roberts, C., and Steinhauser, J. (2022). Climate policy for a net-zero future: ten recommendations for direct air capture. *Environmental Research Letters*, 17(7):074014.

[Span and Wagner, 1996] Span, R. and Wagner, W. (1996). A new equation of state for carbon dioxide covering the fluid region from the triple-point temperature to 1100 K at pressures up to 800 MPa. *Journal of Physical and Chemical Reference Data*, 25.

[Stein, 2022] Stein, T. (2022). Carbon dioxide now more than 50% higher than pre-industrial levels.

[Strassmann et al., 2008] Strassmann, K. M., Plattner, G.-K., and Joos, F. (2008). CO_2 and non-CO_2 radiative forcings in climate projections for twenty-first century mitigation scenarios. *Climate Dynamics*, 33(6):737–749.

[Sun et al., 2021] Sun, X., Zhu, L., Wang, P., Zhao, W., and Chen, X. (2021). CO_2 removal from natural gas by moisture swing adsorption. *Chemical Engineering Research and Design*, 176:162–168.

[Swanson et al., 2012] Swanson, C. E., Elzey, J. W., Hershberger, R. E., Donnelly, R. J., and Pfotenhauer, J. (2012). Thermodynamic analysis of low-temperature carbon dioxide and sulfur dioxide capture from coal-burning power plants. *Physical Review E*, 86(1).

[Tien, 2019] Tien, C. (2019). Introduction. In *Introduction to Adsorption*, pages 1–6. Elsevier.

[UN, 2015] UN (2015). Adoption of the paris agreement, 21st conference of the parties.

[UN, 2022] UN (2022). Statement by the secretary-general at the conclusion of cop27 in sharm el-sheikh.

[Voigt, 2021] Voigt, D. D. C. T. K. F. S. Y. H. W.-T. A. (2021). Roundtable: A global conversation about refrigerant regulations, reductions. *ASHRAE*, 63(6):8.

[von Hippel, 2018] von Hippel, T. (2018). Thermal removal of carbon dioxide from the atmosphere: Energy requirements and scaling issues. *Climatic Change*, 148:491–501.

[Wang et al., 2020] Wang, X., Song, J., Chen, Y., Xiao, H., Shi, X., Liu, Y., Zhu, L., He, Y.-L., and Chen, X. (2020). COsub2/sub absorption over ion exchange resins: The effect of amine functional groups and microporous structures. *Industrial &amp Engineering Chemistry Research*, 59(38):16507–16515.

[Wilcox, 2012] Wilcox, J. (2012). *Carbon Capture*. Springer New York.

[Wilcox et al., 2017] Wilcox, J., Psarras, P. C., and Liguori, S. (2017). Assessment of reasonable opportunities for direct air capture. *Environmental Research Letters*, 12(6):065001.

[Wuebbles and Jain, 2001] Wuebbles, D. J. and Jain, A. K. (2001). Concerns about climate change and the role of fossil fuel use. *Fuel Processing Technology*, 71(1-3):99–119.

[Wurzbacher et al., 2016] Wurzbacher, J. A., Gebald, C., Brunner, S., and Steinfeld, A. (2016). Heat and mass transfer of temperature–vacuum swing desorption for CO_2 capture from air. *Chemical Engineering Journal*, 283:1329–1338.

[Xu et al., 2012] Xu, G., Li, L., Yang, Y., Tian, L., Liu, T., and Zhang, K. (2012). A novel CO_2 cryogenic liquefaction and separation system. *Energy*, 42(1):522–529.

[Yuan et al., 2014] Yuan, L. C., Pfotenhauer, J. M., and Qiu, L. M. (2014). A preliminary investigation of cryogenic CO_2 capture utilizing a reverse Brayton cycle. AIP Publishing LLC.

[Zanganeh et al., 2009] Zanganeh, K. E., Shafeen, A., and Salvador, C. (2009). CO_2 capture and development of an advanced pilot-scale cryogenic separation and compression unit. *Energy Procedia*, 1(1):247–252.

[Zhao et al., 2017] Zhao, R., Deng, S., Liu, Y., Zhao, Q., He, J., and Zhao, L. (2017). Carbon pump: Fundamental theory and applications. *Energy*, 119:1131–1143.

[Zhao et al., 2019] Zhao, R., Liu, L., Zhao, L., Deng, S., Li, S., Zhang, Y., and Li, H. (2019). Thermodynamic exploration of temperature vacuum swing adsorption for direct air capture of carbon dioxide in buildings. *Energy Conversion and Management*, 183:418–426.